PhD thesis

LHC signals and dark matter searches in SO(5)×U(1) gauge-Higgs unification

Takuya Shimotani*

Department of Physics, Osaka University, Toyonaka, Osaka 560-0043, Japan

*shimon@het.phys.sci.osaka-u.ac.jp

Abstract

We construct the $SO(5) \times U(1)$ gauge-Higgs unification with Higgs boson mass $m_H = 126$ GeV on the Randall-Sundrum warped spacetime. We introduce $SO(5) \times U(1)$ gauge fields and fermion multiplets which contain the standard model particles in the bulk region. $SO(5) \times U(1)$ gauge symmetry is broken to $U(1)_{\rm EM}$ by using the Hosotani mechanism as electroweak symmetry breaking mechanism. On the Planck brane there exists brane fermions and brane scalar. The exotic bulk fermions become heavy because of the brane interactions. Dark fermions ($SO(5)$-spinor fermions) are relevant for having the observed unstable Higgs boson. We demonstrate how to determine the relevant parameter sets for $m_H = 126$ GeV. Relevant parameters in this model are determined self-consistently. After we determine the relevant parameters, the global minimum θ_H is determined and all other quantities such as the mass spectra of all KK towers, gauge couplings of all particles, and Yukawa couplings of all fermions are determined. We find that the universal relations that are independent on the detail of the dark fermion sector. The Kaluza-Klein mass spectra of γ, Z, Z_R, top quark, couplings of the first Kaluza-Klein Z boson to quark and Higgs self couplings obey universal relations with Wilson line phase θ_H in the fifth dimension. Higgs cubic and quartic couplings are smaller than those in the standard model. We analyze the decay rates $H \to \gamma\gamma, gg$ and neutral gauge bosons, Z', through dilepton events at LHC. We find that signal strengths of the Higgs decay modes compared to the standard model are $\cos^2\theta_H$. In our model Z' bosons are the first Kaluza-Klein modes $Z_R^{(1)}$, $Z^{(1)}$, and $\gamma^{(1)}$ at TeV scale. An excess of events in the dilepton invariant mass should be observed in the Z' search at the upgraded LHC at 14 TeV. We explore dark matter searches in the $SO(5) \times U(1)$ gauge-Higgs unification. The lightest neutral component of dark fermions becomes the dark matter of the universe. The relic abundance determined by WMAP and Planck data is reproduced with a model with one light and three heavy dark fermions. This model with a mass of the lightest dark fermion from 2.3 TeV to 3.1 TeV is consistent with direct search explored by XENON 100 and LUX experiments. The corresponding Wilson line phase θ_H ranges from 0.097 to 0.074, which is exactly the range explored for Z' search at 14 TeV LHC as well.

Contents

1 Introduction

Results of LHC experiments and realistic models The gauge symmetry is the origin of the forces. The standard model (SM) is the most successful theory. The SM has the $SU(3)_C \times SU(2)_L \times U(1)_Y$ gauge symmetry. The SM is strongly restricted by the gauge symmetry, i.e. mass terms for gauge bosons, and quarks and leptons are forbidden. To generate the mass terms, we introduce a Higgs boson a la the Higgs mechanism. $SU(2) \times U(1)$ gauge symmetry is spontaneously broken by the vacuum expectation value of the Higgs boson. In 2012 the Higgs boson was discovered by LHC experiments[1][2]. All of the particles in the SM are discovered. The Higgs mass is measured to be $m_H = 125.3 \pm 0.4(\text{stat.}) \pm 0.5(\text{syst.})$ GeV and $m_H = 125.36 \pm 0.37(\text{stat}) \pm 0.18(\text{syst})$ GeV by the CMS collaborations and the ATLAS collaboration, respectively[2][3].

There are unsolved problems which we should consider. Firstly the Higgs boson has fine tuning problem. The loop corrections to Higgs mass have the quadratic divergence. To solve this divergence part, we regard the SM as the low energy effective theory, i.e. new physics appears above the certain energy scale. One introduces new physics such as supersymmtery, extra dimensions, compositeness of the Higgs boson and so on above this scale. The new physics predicts new particles such as superpartners, Kaluza-Klein (KK) particles and techni-particles. For example, a model of the extra dimension has the lightest KK particle. If this KK particle is stable, this can become a dark matter candidate. New particles may couple to the SM particle and enhances or suppresses the loop corrections. In other words, new physics may lead to departure from the SM. It is interesting and meaningful to construct a realistic model which reproduce the SM at low energy.

The gauge-Higgs unification The gauge-Higgs unification (GHU) is one of the model beyond the SM. The GHU is formulated in higher dimensional gauge theory. The main feature of GHU is the four dimensional Higgs field which is corresponding to extra dimensional component of the gauge fields. Suppose we consider the Wilson loop operator which integrates gauge fields along direction of extra dimensions. When the extra dimension is non-simply connected space, Wilson loop has non-trivial constant phases which cannot be removed by gauge transformation,

$$e^{i\theta_H} = P \exp\left\{ ig \int_0^{2\pi R} dy \, \langle A_y \rangle \right\}, \tag{1.1}$$

where A_y is the extra dimensional component of gauge fields and θ_H is a constant phase. This constant phase is called the Wilson line phase or the Aharonov-Bohm (AB) phase. The gauge symmetry is dynamically broken by this vacuum expectation value of A_y. This mechanism is called Hosotani mechanism[4][5]. When we apply Hosotani mechanism to the electroweak symmetry breaking, this scenario is called gauge-Higgs unification[6]. A Higgs field appears as a fluctuation of the Wilson line phase, i.e. the Higgs field is the extra dimensional components of the gauge field. GHU is strongly restricted by gauge principle. The 1-loop effective potential and Higgs mass are finite as a consequence of gauge symmetry. In this scenario there appears no fine tuning. This is the main motivation of GHU as a model beyond the SM. Other motivations are to construct the model which only use gauge symmetries as a principle and to discover the extra dimension. One might wonder if sum of the all KK modes in loop corrections has divergence. In GHU 1-loop effective potential and Higgs mass are finite. Therefore physical quantities in the GHU are expected to be finite. This is the interesting feature and we find that loop corrections in $H \to \gamma\gamma$ are finite in $SO(5) \times U(1)$ GHU[7] as well.

The $SO(5) \times U(1)$ gauge-Higgs unification The most realistic model of the GHU is the SO(5)×U(1) GHU[7]-[14]. We introduce $SO(5) \times U(1)$ gauge fields and fermion multiplets which contain the standard model particles in the bulk region. $SO(5) \times U(1)$ gauge symmetry is broken to $U(1)_{\rm EM}$ by using the Hosotani mechanism as electroweak symmetry breaking mechanism. On the Planck brane there exist brane fermions and brane scalar. The exotic bulk fermions in the bulk region become heavy because of the brane interactions. In the original model of the $SO(5) \times U(1)$ GHU, we could not explain the Higgs boson which has been discovered at LHC experiments In the $SO(5) \times U(1)$ GHU Yukawa couplings and Higgs 3-point couplings of gauge bosons are proportional to $\cos\theta_H$. And in the original model of $SO(5) \times U(1)$ GHU the Wilson line phase takes the value $\pi/2$ and all 3-point Higgs couplings of quarks, leptons, W and Z vanish. Therefore Higgs boson becomes stable in the original model of $SO(5) \times U(1)$ GHU. So we should introduce a mechanism that the Higgs become unstable. Then we introduce the additional fermions, which are called dark fermions ($SO(5)$-spinor fermions)[7]. This dark fermion can has the neutral and charged components. In this case the lightest dark fermion can become one of the candidates of the dark matter.

Relevant parameters in this model should be determined self-consistently. We treat the warp factor and the number of the dark fermions as free parameters. We choose the

global minimum in the effective potential tentatively to determine self-consistently. Then we calculate the other relevant parameters and determine the Higgs mass. If the obtained Higgs mass is smaller (larger) than 126 GeV, we reiterate the same procedure with smaller (larger) tentative value of the global minimum. After we determine the relevant parameters, the global minimum θ_H is determined and all other quantities such as the mass spectra of all KK towers, gauge couplings of all particles, and Yukawa couplings of all fermions are determined.

We find that the universal relation which is independent on the details in the dark fermion sector. The universality relations appear among θ_H, the KK mass, the masses of $Z^{(1)}$, $\gamma^{(1)}$ and $t^{(1)}$, couplings of $Z^{(1)}\bar{q}q$ and the Higgs self-couplings[7]. Once the θ_H is determined from, say, $Z^{(1)}$ mass, we can determine other quantities, $\gamma^{(1)}$ mass , the Higgs self-couplings and so on. If one finds the value of $m_{Z^{(1)}}(\theta_H)$ from experiments, θ_H is determined and other quantities are predicted. Our Higgs cubic and quartic couplings are smaller than those in the SM.

We analyze the Higgs decay, $H \to \gamma\gamma$, and Z' search[7][13]. We can know the Wilson line phase θ_H from the analysis by using universality. We find that in signal strength of $H \to \gamma\gamma$, dominant factor of deviation from the SM is $\cos^2\theta_H$ which comes from the Higgs couplings. First exited KK modes of Z boson $Z^{(1)}$, photon $\gamma^{(1)}$, the lowest mode of Z_R and $Z_R^{(1)}$ have TeV scale mass in the $SO(5) \times U(1)$ gauge-Higgs unification. These massive neutral gauge bosons appear as Z' boson. Z' in the $SO(5) \times U(1)$ GHU is strongly coupled with right handed fermions so that Z' resonance has large width. In the region $\theta_H < 0.13$, $SO(5) \times U(1)$ GHU is consistent with the $H \to \gamma\gamma$ and Z' search at 8 TeV LHC experiments. And we predict Z' are discovered in the 14 TeV LHC experiments.

In addition to the collider experiments we examine the implication to the dark matter problem. We assign the $U(1)$ charge such that the dark fermions contain the neutral components[14]. In the $SO(5) \times U(1)$ GHU the number of dark fermions is conserved so that the lightest neutral dark fermions become stable. In the non-degenerate case of one lighter neutral dark fermion and three heavier neutral dark fermions, we can explain the relic density. We also examine the direct detection. In the region $\theta_H = 0.097 - 0.074$, our model is consistent with the experiments of the relic density and the direct detection. Especially for the direct detection the model indicates dark matter is expected to be discovered in the next LUX experiments.

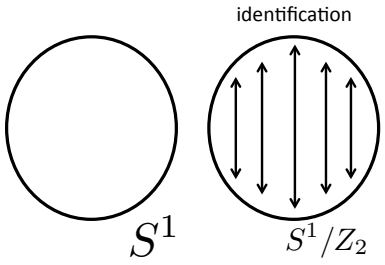

Figure 1: The left panel shows S^1. The right panel shows the identification of the S^1/Z_2.

Extra dimension The most simplest case is $M^4 \times S^1$ in the model of the extra dimension. The characteristic quantity of extra dimension is radius R. Wave functions of fields on the S^1 satisfy equations of motion. The wave function is expanded by the complete set. We get wave functions and call KK mode for each mode. And also the equations of motion give us the masses of each mode of the fields. Characteristic mass scale is $1/R$. This is called KK mass. However on the $S^1 \times M^4$ fermions are vector-like so that the SM cannot be not reproduced. To have chiral fermions, we introduce the orbifold structure S^1/Z_2 in which the upper side of S^1 is identified with the lower side of S^1, Fig.1. We introduce the boundary conditions for a line segment. We can impose Dirichlet boundary condition (fixed boundary condition), Neumann boundary condition and so on. Four dimensional spacetime of end points are called the branes. And the other part is called the bulk. When we impose Neumann boundary condition at both end points, the wave function is cosine function because end points are not fixed. When we impose Dirichlet boundary condition at both end points, the wave function is sine function because end points are fixed. This sine function has no zero mode. If left- and right-handed fermions are imposed by Neumann boundary condition and Dirichlet boundary condition, respectively, only the left handed fermions has the lowest mode. We can consider more complicated case. The Randall-Sundrum warped spacetime is a famous spacetime, Fig.2 [15]. Characteristic factor is called warp factor which connects the TeV scale to the Planck scale. The fine tuning problem is solved by this warp factor.

Contents of this paper In Sec. 2 we have the brief review of the Hosotani mechanism for $SU(N)$ gauge theory on the $M^4 \times S^1$. In Sec. 3 the action of the $SO(5) \times U(1)$ GHU is given. In Sec. 4 we calculate effective potentials V_{eff} and determine global minimum

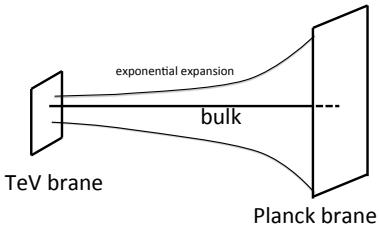

Figure 2: This show the Randall-Sundrum warped spacetime. Horizontal axis is fifth dimensional direction. Planes mean four dimension. Four dimensional coordinates expand exponentially from TeV brane to Planck brane.

of the effective potential and Higgs mass. And we find universality which is independent of the detail in the dark fermion sector. In Sec. 5 we discuss Higgs decay $H \to \gamma\gamma, gg$ and behaviors of the couplings for each KK mode. And we examine the Z' search. We calculate dilepton process at tree level for 8 TeV and 14 TeV LHC experiments. In Sec. 6 we introduce the scenario which regard dark fermions as one of the candidates of dark matter. We calculate the relic density and the direct detections of dark fermions . We find that in our model we have a parameter region which is consistent with the experiments of the relic density and direct search.

2 Hosotani mechanism

We shortly review Hosotani mechanism[4][5]. This section is based on [5]. Hosotani mechanism is the spontaneously symmetry breaking mechanism in higher dimensional gauge theory. When the space is not simply connected, the Wilson loop can have constant phase. Because the Wilson loop is gauge invariant quantity, this phase cannot remove. This phase is dynamically determined by the 1-loop effective potential. Higgs mass is finite because of gauge symmetry. This phase give fermion mass and gauge boson mass at quantum level. Therefore fine tuning problem is solved.

In this section the constant phase appears from Wilson loop. By using background gauge method we calculate the 1-loop effective potential for Wilson line phase.

2.1 Boundary conditions and equivalence class

Let us first consider $SU(N)$ gauge theory in the five dimensions. We mainly focus on the gauge field. The fifth dimension is S^1 compactification which has radius R. We denote the four dimensional Minkowski coordinate x^μ, the fifth dimensional coordinate y. We identify y and $y + 2\pi R$ with boundary conditions U,

$$A_M(x, y + 2\pi R) \;=\; U A_M(x, y) U^\dagger, \tag{2.1}$$

where $T[U]$ means fundamental or adjoint representation. We consider the gauge transformation,

$$A_\mu(x, y) \;\to\; A'_M(x, y) = \Omega(x, y) A_M(x, y) \Omega^\dagger(x, y) - \frac{i}{g} \Omega(x, y) \partial_M \Omega^\dagger(x, y), \tag{2.2}$$

where A'_M satisfies the new boundary condition U'. Now we discuss the relation between boundary conditions U and U'. By using the gauge transformation Ω, one finds the relation,

$$U' = \Omega(x, y + 2\pi R) U \Omega(x, y). \tag{2.3}$$

If $\Omega(x, y)$ obeys

$$\Omega^\dagger(x, y + 2\pi R) \partial_M \Omega(x, y + 2\pi R) U = U \Omega(x, y) \partial_M \Omega(x, y), \tag{2.4}$$

U' is independent on coordinates. Because the boundary conditions U and U' are related by the gauge transformation $\Omega(x, y)$, these boundary conditions satisfied with (2.4) are equivalent,

$$U \sim U'. \tag{2.5}$$

We call this relation (2.5) equivalence class. Not all boundary conditions U are not independent. Some boundary conditions are related to other boundary condition by gauge transformations. We have the residual gauge invariance which is unchanged boundary conditions ($U = U'$),

$$\Omega(x, y + 2\pi R) = U \Omega(x) U^\dagger, \tag{2.6}$$

where $\Omega(x, y)$ is not single-valued unless $[\Omega(x, y), U] = 0$.

2.2 Vacuum configuration and the Wilson line phase

In simply connected space the vacuum expectation values of gauge fields can gauge away, while in non-simply connected space gauge fields can have the non-vanishing expectation value. We consider the vacuum configuration of the classical case $\langle F_{MN}\rangle = 0$. It follows that,

$$\langle A_M\rangle = -\frac{i}{g}V^\dagger(x,y)\partial_M V(x,y). \tag{2.7}$$

We use the boundary condition (2.1),

$$V^\dagger(x,y+2\pi R)\,\partial_M V(x,y+2\pi R)\,U = U\,V^\dagger(x,y)\partial_M V(x,y). \tag{2.8}$$

We transform eq.(2.7) by gauge transformation $\Omega(x,y)$,

$$\langle A_M\rangle \to \langle A'_M\rangle = -\frac{i}{g}(\Omega V^\dagger)\partial_M(V\Omega^\dagger). \tag{2.9}$$

V is not unique. CV ($CC^\dagger = 1$) is also satisfied with (2.7), C is a constant unitary matrix. If $\Omega(x,y) = V(x,y)$, $\langle A'_M\rangle$ is transformed to zero. The boundary condition is changed to

$$U' = V(x,y+2\pi R)\,U\,V(x,y)^\dagger. \tag{2.10}$$

(2.8) indicates U' is independent on the coordinates. Therefore we have the equivalence class,

$$\left(U;\langle A_M\rangle = -\frac{i}{g}V^\dagger\partial_M V\right) \sim (U';\langle A_M\rangle = 0). \tag{2.11}$$

This means A_M is fixed when the boundary condition U is fixed. We cannot discuss A_M and the boundary condition independently.

Let us introduce the path-ordered Wilson loop with contour C,

$$W^{(0)}[x,y;C] = P\exp\left\{ig\int_{x,y}^{x,y+2\pi R} A_M\,dx^M\right\}. \tag{2.12}$$

Generally $W^{(0)}[x,y;C]$ is not gauge covariant because $\Omega(x,y) \neq \Omega(x,y+2\pi R)$. So we redefine,

$$W[x,y;C] = W^{(0)}[x,y;C]U, \tag{2.13}$$

where U is introduced in eq.(2.1). Thus $W[x,y;C]$ is transformed,

$$\begin{aligned} W[x,y;C] \to W'[x,y;C] &= \Omega(x,y)W^{(0)}[x,y,\ C]\Omega^\dagger(x,y+2\pi R)U \\ &= \Omega(x,y)W[x,y;C]\Omega^\dagger(x,y). \end{aligned} \tag{2.14}$$

Eigenvalues of $W[x,y;C]$ are gauge invariant. We consider the vacuum configuration $F_{MN}=0$. In this time $W[x,y;C]$ is given by

$$W[x,y;C] \;=\; V^\dagger(x,y)V(x,y+2\pi R)U. \tag{2.15}$$

We transform (2.15) with the gauge transformation $\Omega(x,y)=V(x,y)$ which changes the boundary condition,

$$W'[x,y;C]=V(x,y+2\pi R)UV^\dagger(x,y)=V(x,y)W[x,y;C]V^\dagger(x,y). \tag{2.16}$$

This means $W'[x,y;C]=U'$ in (2.10). Thus U' and $W[x,y;C]$ have the same eigenvalues. Since U' is independent on the coordinates, the eigenvalues of $W[x,y;C]$ are also independent on coordinates. This eigenvalues are called the Wilson line phase. In $SU(N)$ gauge theory,

$$\left\{ e^{i\theta_k^a}, \sum_{k=1}^{N}\theta_k^a = 0 \ (\mathrm{mod}\, 2\pi) \qquad (a=1\sim n) \right\}, \tag{2.17}$$

where θ_k^a is the Wilson line phase. In the non-simply connected space the gauge field can contain this Wilson line phase. This Wilson line phase cannot be gauged away in the equivalence class. We summarize the relation between the boundary conditions and the gauge transformations in Fig. 2.2.

2.3 Effective Potential

Let us calculate the 1-loop effective potential by using background field method in the S^1 compactification. Lagrangian is,

$$\begin{aligned} L &= -\frac{1}{2}\mathrm{Tr}F_{MN}F^{MN}, \\ F_{MN} &= \partial_M A_N - \partial_N A_M + ig[A_M, A_N], \end{aligned} \tag{2.18}$$

where ζ_M is external field. The gauge fixing function is,

$$F[A]=D_M(\zeta)A^M=\partial_M A^M + ig[\zeta_M, A^M]. \tag{2.19}$$

Faddeev-Popov operator is,

$$M_{\alpha\beta}=\frac{\delta F_\alpha}{\delta A_\gamma^M}D^M(A)_{\gamma\beta}=D_M(\zeta)_{\alpha\gamma}D^M(A)_{\gamma\beta}, \tag{2.20}$$

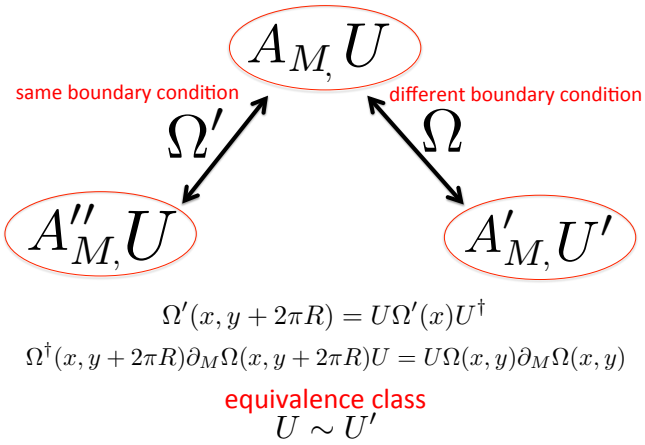

Figure 3: Ω is the gauge transformation which change the boundary condition. Ω' is the gauge transformation which does not change the boundary condition. All gauge fields in this figure contain the same Wilson line phase in the non-simply connected space.

where η is the ghost field. The effective Lagrangian is,

$$\begin{aligned} L_{\rm eff}[A,\eta,\bar{\eta}] &= -\frac{1}{2}{\rm Tr}F_{MN}F^{MN} \\ &\quad -\frac{1}{\alpha}{\rm Tr}\{D_M(\zeta)A^M\}^2 - {\rm Tr}\,\bar{\eta}D_M(\zeta)D^M(A)\eta. \end{aligned} \tag{2.21}$$

To get the 1-loop effective potential we divide classical parts and quantum parts which is left quadratic parts. We can use Euler-Lagrange equation for classical parts. We use gauge fixing condition,

$$\begin{aligned} A_M = A^0_M + A^q_M, \quad \langle A_M\rangle = A^0_M, \\ F^0_{MN} = \partial_M A^0_N - \partial_N A^0_M + ig[A^0_M, A^0_N], \\ D^0_M = D_M(A^0), \bar{D}_M = D_M(\zeta). \end{aligned} \tag{2.22}$$

$$\begin{aligned} L_{\rm eff}[A^0 + A^q, \eta, \bar{\eta}] \supset & -\frac{1}{2}{\rm Tr}\,(D^0_M A^q_N - D^0_N A^q_M)(D^{0M}A^{qN} - D^{0N}A^{0M}) \\ & -ig{\rm Tr}\,F^{0MN}[A^q_M, A^q_N] \\ & -\frac{1}{\alpha}{\rm Tr}\{\bar{D_M}A^{qM}\}^2 - {\rm Tr}\,\bar{\eta}\bar{D}_M D^{0M}\eta. \end{aligned} \tag{2.23}$$

We integrate by part and use $[D^0_M, D^0_N]A^{qM} = ig[F^0_{MN}, A^{qM}]$,

$$\begin{aligned} L_{\rm eff} \sim & \ {\rm Tr}\,A^q_M D^0_N D^{0N}A^{qM} - 2ig{\rm Tr}\,F^0_{MN}[A^{qM}, A^{qN}] \\ & -{\rm Tr}\,\bar{\eta}\bar{D}_M D^{0M}\eta + {\rm Tr}(D^0_M A^{qM})^2 - \frac{1}{\alpha}{\rm Tr}(\bar{D}_M A^{qM})^2. \end{aligned} \tag{2.24}$$

Then we take $\zeta = A^0$ and $\alpha = 1$,

$$L_{\text{eff}} \sim -\text{Tr} A^{qM} M^g_{MN} A^{qN} - \text{Tr}\,\bar{\eta} M^{gh} \eta \tag{2.25}$$

$$M^g_{MN} = -g_{MN} D^0_\rho D^{0\rho} - 4igF^0_{MN} \tag{2.26}$$

$$M^{gh} = D^0_\rho D^{0\rho}. \tag{2.27}$$

Therefore we get the 1-loop effective potential for A^0,

$$\begin{aligned} V_{\text{eff}}[A^0]^g &= -\tfrac{i}{2}\,\text{Tr}\ln M^g, \\ V_{\text{eff}}[A^0]^{gh} &= i\,\text{Tr}\ln M^{gh}. \end{aligned} \tag{2.28}$$

In the case of $F^0_{MN} = 0$,

$$V_{\text{eff}}[A^0]^{g+gh} = -(d-2)\frac{i}{2}\text{Tr}\ln D_M(A^0) D^M(A^0). \tag{2.29}$$

In the fermion part, contributions of fundamental representation $fund$ and adjoint representation adj are

$$\begin{aligned} D^f_M(A^0)\psi_{fund} &= (\partial_M + igA^0_M)\psi, \\ D^{adj}_M\,\psi_{ad} &= \partial_M + ig[A^0_M, \psi_{ad}], \\ V_{\text{eff}}[A^0]^{\text{fermion}} &= i\text{Tr}\ln\{i\gamma^M D_M(A^0) - m\}. \end{aligned} \tag{2.30}$$

For massless Dirac fermion,

$$V_{\text{eff}}[A^0]^{\text{fermion}} = 2^{d/2} i\text{Tr}\ln D_M(A^0) D^M(A^0). \tag{2.31}$$

Firstly we calculate the contribution of the fermion with fundamental representation,

$$\begin{aligned} V_{\text{eff}}[\theta]^{fund} &= 2^{5/2} i\text{Tr}\ln(-i\partial_M + gA_M)^2 \\ &= 2^{5/2}\frac{i}{2}\frac{1}{2\pi R}\sum_{n=-\infty}^{+\infty}\int\frac{d^4p}{(2\pi)^4}\text{Tr}\ln\{p_0^2 - p_1^2 - p_2^2 - p_3^2 - (\omega_n - gA_y)^2\} \\ &= \frac{2^{5/2}}{4\pi R}\sum_{j=1}^{N}\sum_{n=-\infty}^{\infty}\int\frac{d^4p}{(2\pi)^4}\ln\left\{\mathbf{p}^2 + \left(\omega_n - \frac{\theta_j}{2\pi R}\right)^2\right\}, \end{aligned} \tag{2.32}$$

where $\omega_n = n/R$. In the second line of eq.(2.32), we get rid of constant term,

$$\begin{aligned} \sum_{n=-\infty}^{\infty}\ln\{(2\pi n - x)^2 + E^2\} &= \ln(1 - e^{E+ix})(1 - e^{-E-ix}) \\ &\quad + (x - \text{indpendent}). \end{aligned} \tag{2.33}$$

To use the gamma function,

$$\begin{aligned} V_{\rm eff}^{fund} &= -\frac{2^{5/2}}{4\pi R}\sum_{j=1}^{N}\frac{2}{(4\pi)^2}\frac{1}{\Gamma(2)}\int_0^\infty dp\, p^3\{\ln\left(1-e^{2\pi Rp+i\theta_j}\right)+\ln\left(1-e^{2\pi Rp-i\theta_j}\right)\} \\ &= \frac{2^{5/2}\Gamma(2)}{(2\pi R)^5\pi^{5/2}}\sum_{j=1}^{N}\sum_{n=1}^{\infty}\frac{1}{n^5}\cos n\theta_j. \end{aligned} \tag{2.34}$$

In the similar way we can get the contributions of fermions for adjoint representation,

$$V_{\rm eff}^{adj} = \frac{2^{5/2}\Gamma(2)}{(2\pi R)^5\pi^{5/2}}\sum_{j,k=1}^{N}\sum_{n=1}^{\infty}\frac{1}{n^5}\cos n(\theta_j-\theta_k). \tag{2.35}$$

Finally we get contributions of gauge fields and ghost fields,

$$V_{\rm eff}^{g+gh} = -\frac{2^{5/2}\Gamma(2)}{(2\pi R)^5\pi^{5/2}}\sum_{j,k=1}^{N}\sum_{n=1}^{\infty}\frac{1}{n^5}\cos n(\theta_j-\theta_k). \tag{2.36}$$

Here we consider the dependence of boundary conditions for 1-loop effective potential. We consider the following gauge trans formation,

$$A_M^{0'} = \Omega A_M^0\Omega^\dagger - \frac{i}{g}\Omega\partial_M\Omega^\dagger. \tag{2.37}$$

Euler-Lagrange equation for gauge fields and gauge fixing condition are,

$$\begin{aligned} D^M(A^0)F_{MN}(A^0) = 0, \\ D^M(A^0)A_M^0 = 0. \end{aligned} \tag{2.38}$$

The gauge fixing condition (Second line of eq.(2.38)) is not gauge invariant satisfied for eq.(2.37). In this time we consider the gauge fixing condition is gauge invariant and satisfied with

$$D_M(A^0)\partial_M\Omega^\dagger\Omega = 0. \tag{2.39}$$

Thus the gauge fixing term is gauge invariant with $A'_M = A_M^{0'} + A_M^{q'}$,

$$\begin{aligned} F'[A'] &= D^M(A^{0'})A'_M \\ &= \Omega\left\{D^M(A^0)A_M - \frac{i}{g}D^M(A^0)\partial_M\Omega^\dagger\Omega\right\}\Omega^\dagger \\ &= \Omega F[A]\Omega^\dagger. \end{aligned} \tag{2.40}$$

Therefore, the 1-loop effective potential is unchanged for both boundary conditions U and U',

$$V_{\rm eff}[A^0;U] = V_{\rm eff}[A^{0'};U']. \tag{2.41}$$

3 Model

In this section we define $SO(5)\times U(1)$ GHU [7]-[14]. $SO(5)\times U(1)$ GHU model is the most realistic model which reconstructs the SM. Firstly we introduce the $SU(3)_C \times SO(5) \times U(1)_X$ gauge symmetry on the Randall-Sundrum warped space-time. Then we discuss the symmetry breaking. Secondly we introduce the 5 dimensional fermions. Exotic fermions become heavy because of the brane interactions. We introduce the additional fermions, which are called the dark fermions ($SO(5)$-spinor fermions). We explain the relevant parameters in the next section.

3.1 Gauge fields in the $SO(5) \times U(1)$ GHU

3.1.1 Gauge symmetry

We introduce the $SU(3)_C \times SO(5) \times U(1)_X$ gauge symmetry on the Randall-Sundrum warped spacetime [15]. Fifth dimensional space is the line segment with length L. The boundary of the fifth dimensional space is called the brane and the other region is called the bulk. We denote y is the fifth dimensional coordinate. An four dimensional part of end point at $y = 0$ is called the Planck brane, the other end point at $y = L$ is called the TeV brane. The metric of the Randall-Sundrum warped spacetime is given by

$$ds^2 = G_{MN}dx^M dx^N = e^{-2\sigma(y)}\eta_{\mu\nu}dx^\mu dx^\nu + dy^2 \ , \tag{3.1}$$

where $\eta_{\mu\nu} = \mathrm{diag}(-1, 1, 1, 1)$, $\sigma(-y) = \sigma(y)$, $\sigma(y + 2L) = \sigma(y)$ and $\sigma(y) = k|y|$ for $|y| \leq L$. k is the curvature, which has the value from 10^4 TeV to 10^7 TeV. The characteristic factor $z_L = e^{kL}$ is called the warp factor, which has the value from 10^4 to 10^7. This warp factor connects between the weak scale and Planck scale. The cosmological constant is given by $\Lambda = -6k^2$. We rewrite the metric with the conformal coordinate $z = e^{ky}$,

$$ds^2 = \frac{1}{z^2}\Big(\eta_{\mu\nu}dx^\mu dx^\nu + \frac{dz^2}{k^2}\Big) \ . \tag{3.2}$$

This form is useful to calculate the wave functions. The KK mass scale is given by $m_{\mathrm{KK}} = \pi k/(z_L - 1) \sim \pi k z_L^{-1}$. In this paper we focus on $m_{\mathrm{KK}} = 4 - 10$ TeV.

There exist the $SU(3)_C \times SO(5) \times U(1)_X$ gauge fields in the bulk region. $SU(3)_C$ gauge fields become gluon fields in the 4 dimensions. Because of introducing the 4 dimensional Higgs doublet, we introduce the $SO(5) \times U(1)_X$ gauge fields. We note that $SU(3)$ GHU model does not obtain the Weinberg angle. The bulk part of the action is given by

$$S^{\mathrm{gauge}}_{\mathrm{bulk}} = \int d^5x\sqrt{-G}\Big[-\mathrm{tr}\Big(\frac{1}{4}F^{(A)MN}F^{(A)}_{MN} + \frac{1}{2\xi_A}(f^{(A)}_{\mathrm{gf}})^2 + \mathcal{L}^{(A)}_{\mathrm{gh}}\Big)$$

$$-\Big(\frac{1}{4}F^{(B)MN}F^{(B)}_{MN}+\frac{1}{2\xi_B}(f^{(B)}_{\rm gf})^2+\mathcal{L}^{(B)}_{\rm gh}\Big)$$
$$-{\rm tr}\,\Big(\frac{1}{2}F^{(G)MN}F^{(G)}_{MN}+\frac{1}{\xi_C}(f^{(G)}_{\rm gf})^2+\mathcal{L}^{(G)}_{\rm gh}\Big)\Big], \tag{3.3}$$

where A_M, B_M and G_M ($M=\mu$ and y) are $SO(5)$, $U(1)_X$ and $SU(3)_C$ gauge fields, respectively. Field strengths are given by

$$F^{(A)}_{MN} = \partial_M A_N-\partial_N A_M-ig_A\big[A_M,A_N\big], \tag{3.4}$$
$$F^{(B)}_{MN} = \partial_M B_N-\partial_N B_M, \tag{3.5}$$
$$F^{(G)}_{MN} = \partial_M G_N-\partial_N G_M-ig_C[G_M,G_N]. \tag{3.6}$$

g_A and g_C are $SO(5)$ and $SU(3)_C$ charge, respectively. We denote the g_B is the $U(1)_X$ charge. We take the gauge fixing function,

$$f^{(A)}_{\rm gf}=z^2\big\{\eta^{\mu\nu}\mathcal{D}_\mu A_\nu+\xi_A k^2 z\mathcal{D}^c_z(A^q_z/z)\big\} \tag{3.7}$$

with a background field A^c_z ($A_z=A^c_z+A^q_z$), $B^c_z=G^c_z=0$.

Now we discuss the symmetry breaking. $SO(5)\times U(1)_X$ gauge symmetry breaks to the $SO(4)\times U(1)$ gauge symmetry by the boundary conditions at $y_0=0$ and $y_1=L$,

$$\begin{pmatrix}A_\mu\\A_y\end{pmatrix}(x,y_j-y)=P_{\rm vec}\begin{pmatrix}A_\mu\\-A_y\end{pmatrix}(x,y_j+y)P^{-1}_{\rm vec},$$
$$\begin{pmatrix}B_\mu\\B_y\end{pmatrix}(x,y_j-y)=\begin{pmatrix}B_\mu\\-B_y\end{pmatrix}(x,y_j+y),$$
$$\begin{pmatrix}G_\mu\\G_y\end{pmatrix}(x,y_j-y)=\begin{pmatrix}G_\mu\\-G_y\end{pmatrix}(x,y_j+y),$$
$$P_{\rm vec}={\rm diag}\,(-1,-1,-1,-1,+1) \tag{3.8}$$

Four dimensional $SO(4)$ part and five dimensional $SO(5)/SO(4)$ part of the gauge field A_M have parity even whereas four dimensional $SO(5)/SO(4)$ part and five dimensional $SO(4)$ part of the gauge field A_M have parity odd. By this boundary condition $SO(5)$ symmetry breaks to $SO(4)$, which is equivalent to the $SU(2)_L\times SU(2)_R$. $SU(2)_L\times SU(2)_R$ indicates that the Peskin-Takeuchi T parameter is zero. $SU(2)_R\times U(1)$ symmetry is spontaneously broken to $U(1)_Y$ by the brane scalar $\hat{\Phi}$. This brane scalar lives on the Planck brane. The vacuum expectation value of the brane scalar is $\langle\hat{\Phi}\rangle\gg m_{\rm KK}$. At this time we have the massive charged and neutral gauge bosons which come from the $SU(2)_R\times U(1)_X$.

We call charged gauge boson $W_R^{\pm}$ and neural gauge boson Z_R. Massless neutral gauge boson corresponds to $U(1)_Y$ field. And then we have the SM symmetry, $SU(2)_L \times U(1)_Y$ symmetry. $SU(2)_L \times U(1)_Y$ symmetry is spontaneously broken to $U(1)_{\rm EM}$ by the Hosotani mechanism. $SU(2)_L \times U(1)_Y$ symmetry is unbroken at flat spacetime which is not Randall-Sundrum warped spacetime. The $SO(5)$ gauge fields A_M are decomposed as

$$A_M = \sum_{a_L=1}^{3} A_M^{a_L} T^{a_L} + \sum_{a_R=1}^{3} A_M^{a_R} T^{a_R} + \sum_{\hat{a}=1}^{4} A_M^{\hat{a}} T^{\hat{a}}, \tag{3.9}$$

where $T^{a_L,a_R}(a_L, a_R = 1,2,3)$ and $T^{\hat{a}}(\hat{a} = 1,2,3,4)$ are the generators of $SO(4) \simeq SU(2)_L \times SU(2)_R$ and $SO(5)/SO(4)$, respectively. Note that generators of the $SU(2)_L \times U(1)_Y$ gauge symmetry are mixed generators of $SO(5) \times U(1)$ gauge symmetry by the Wilson line phase θ_H after the electroweak symmetry breaking, Appendix B.

3.1.2 Four dimensional Higgs boson

The $SO(5)/SO(4)$ coset part of the gauge field A_y contains four dimensional Higgs doublet. Without loss of generality the zero mode of $A^{\hat{4}}$ component of A_y can has vacuum expectation value when the EW symmetry is spontaneously broken. The zero modes of $A_y^{\hat{a}}$ (a = 1,2,3) are absorbed by W and Z bosons. The four-dimensional neutral Higgs field $H(x)$ appears as a fluctuation mode of the Wilson line phase,

$$\begin{aligned}
&A_y^{\hat{4}}(x,y) = \big\{\theta_H f_H + H(x)\big\}\tilde{u}_H(y) + \cdots \ , \\
&\exp\left\{\frac{i}{2}\theta_H \cdot 2\sqrt{2}T^{\hat{4}}\right\} = \exp\left\{ig_A \int_0^L dy \, \langle A_y \rangle\right\} \ , \\
&f_H = \frac{2}{g_A}\sqrt{\frac{k}{z_L^2 - 1}} = \frac{2}{g_w}\sqrt{\frac{k}{L(z_L^2 - 1)}} \ ,
\end{aligned} \tag{3.10}$$

where $g_w = g_A/\sqrt{L}$ is the dimensionless 4 dimensional $SU(2)_L$ coupling. After the KK decomposition we get the wave function of the four-dimensional Higgs boson,

$$\tilde{u}_H(y) = \sqrt{\frac{2k}{z_L^2 - 1}} e^{ky}, \quad 0 \le y \le L, \tag{3.11}$$

where $\tilde{u}_H(-y) = \tilde{u}_H(y) = \tilde{u}_H(y + 2L)$.

3.1.3 KK decomposition of the gauge fields

The gauge fields are expanded by the terms of Bessel functions,

$$
\begin{aligned}
&C(z;\lambda) = \frac{\pi}{2}\lambda z z_L F_{1,0}(\lambda z, \lambda z_L) \ , \quad C'(z;\lambda) = \frac{\pi}{2}\lambda^2 z z_L F_{0,0}(\lambda z, \lambda z_L) \ , \\
&S(z;\lambda) = -\frac{\pi}{2}\lambda z F_{1,1}(\lambda z, \lambda z_L) \ , \quad S'(z;\lambda) = -\frac{\pi}{2}\lambda^2 z F_{0,1}(\lambda z, \lambda z_L) \ , \\
&\hat{S}(z;\lambda) = \frac{C(1;\lambda)}{S(1;\lambda)} S(z;\lambda) \ , \\
&F_{\alpha,\beta}(u,v) = J_\alpha(u)Y_\beta(v) - Y_\alpha(u)J_\beta(v) \ .
\end{aligned}
\tag{3.12}
$$

where $m = \lambda k$. These functions satisfy

$$
\begin{aligned}
&C(z_L;\lambda) = z_L \ , \quad C'(z_L;\lambda) = 0 \ , \quad S(z_L;\lambda) = 0 \ , \quad S'(z_L;\lambda) = \lambda \ , \\
&CS' - SC' = \lambda z \ .
\end{aligned}
\tag{3.13}
$$

Four dimensional components of the gauge fields are expanded by $C(z;\lambda)$ or $S(z;\lambda)$. These functions depend on the boundary condition. $C(z;\lambda)$ is corresponding to the Neumann condition and $S(z;\lambda)$ is corresponding to the Dirichlet boundary condition at TeV brane. At large mass, wave functions of the $C(z;\lambda)$ and $S(z;\lambda)$ localize the TeV brane. Therefore large KK modes of the gauge bosons have the wave functions which is localize the TeV brane.

We determine the spectrum and wave function of the KK mode of gauge fields. We introduce the convenient gauge because of the brane interaction at Planck brane. We call the twisted gauge. This gauge conserve the boundary condition at the TeV brane, whereas background gauge field is transformed to zero at the Planck brane. The twisted gauge is given by a gauge transformation,

$$
\begin{aligned}
\Omega &= \exp\left\{ i g_A \theta_H f_H T^{\hat{4}} \int_y^L dy\, u_H(y) \right\} \\
&= \exp\left\{ i\theta_H \frac{z_L^2 - z^2}{z_L^2 - 1} \sqrt{2}\, T^{\hat{4}} \right\} \quad \text{for } 1 \le z \le z_L \ .
\end{aligned}
\tag{3.14}
$$

As we mentioned in the previous section, some boundary conditions are related to other boundary condition by gauge transformations. This gauge transformation change the orbifold boundary conditions,

$$
\tilde{P}_j = \Omega(y_j - y) P_0 \Omega(y_j + y)^{-1}, \tag{3.15}
$$

where $i = 0, 1$. At $z = z_L$, $\Omega(z_L) = 1$. This means the boundary condition at the TeV brane is unchanged. The orbifold boundary condition matrix P_0 changes,

$$\tilde{P}_0^{\rm vec} = \begin{pmatrix} -1 & & & & \\ & -1 & & & \\ & & -1 & & \\ & & & -\cos 2\theta_H & \sin 2\theta_H \\ & & & \sin 2\theta_H & \cos 2\theta_H \end{pmatrix} . \tag{3.16}$$

Under the twisted gauge, $A_\mu(x,z)$ and $B_\mu^X(x,z)$ are expanded in KK towers.

$$\begin{aligned} &\tilde{A}_\mu(x,z) + \frac{g_B}{g_A} B_\mu(x,z) T_B \\ &\quad = \hat{W}_\mu^- + \hat{W}_\mu^+ + \hat{Z}_\mu + \hat{A}_\mu^\gamma + \hat{W}_{R\mu}^- + \hat{W}_{R\mu}^+ + \hat{Z}_{R\mu} + \hat{A}_\mu^{\hat{4}} , \end{aligned} \tag{3.17}$$

$$\hat{W}_\mu^\mp = \sum_n W_\mu^{(n)\mp}(x) \left\{ h^L_{W^{(n)}} \frac{T^{1_L} \mp i T^{2_L}}{\sqrt{2}} + h^R_{W^{(n)}} \frac{T^{1_R} \mp i T^{2_R}}{\sqrt{2}} + \hat{h}_{W^{(n)}} \frac{T^{\hat{1}} \mp i T^{\hat{2}}}{\sqrt{2}} \right\},$$

$$\hat{Z}_\mu = \sum_n Z_\mu^{(n)}(x) \left\{ h^L_{Z^{(n)}} T^{3_L} + h^R_{Z^{(n)}} T^{3_R} + \hat{h}_{Z^{(n)}} T^{\hat{3}} + \frac{g_B}{g_A} h^B_{Z^{(n)}} T_B \right\},$$

$$\hat{A}_\mu^\gamma = \sum_n A_\mu^{\gamma(n)}(x) \left\{ h^L_{\gamma^{(n)}} T^{3_L} + h^R_{\gamma^{(n)}} T^{3_R} + \frac{g_B}{g_A} h^B_{\gamma^{(n)}} T_B \right\},$$

$$\hat{W}_{R\mu}^\mp = \sum_n W_{R\mu}^{(n)\mp}(x) \left\{ h^L_{W_R^{(n)}} \frac{T^{1_L} \mp i T^{2_L}}{\sqrt{2}} + h^R_{W_R^{(n)}} \frac{T^{1_R} \mp i T^{2_R}}{\sqrt{2}} \right\},$$

$$\hat{Z}_{R\mu} = \sum_n Z_{R\mu}^{(n)}(x) \left\{ h^L_{Z_R^{(n)}} T^{3_L} + h^R_{Z_R^{(n)}} T^{3_R} + \frac{g_B}{g_A} h^B_{Z_R^{(n)}} T_B \right\},$$

$$\hat{A}_\mu^{\hat{4}} = \sum_n A_\mu^{\hat{4}(n)}(x) \hat{h}_{A^{\hat{4}(n)}} T^{\hat{4}},$$

$$\hat{W}^\pm = \frac{\hat{W}^1 \mp i \hat{W}^2}{\sqrt{2}} , \quad \hat{W}_R^\pm = \frac{\hat{W}_R^1 \mp i \hat{W}_R^2}{\sqrt{2}} . \tag{3.18}$$

where $U(1)_X$ generator T_B is satisfied with $\mathrm{Tr}\, {T_B}^2 = 1$, $\mathrm{Tr}\, T_B T^\alpha = 0$ and $\mathrm{Tr}\, T^\alpha T^\beta = \delta^{\alpha\beta}$. The lowest modes of the $\hat{W}^\pm, \hat{Z}$ and $\hat{A}^\gamma$ towers are $W^\pm$ boson, Z boson and photon, respectively. The other towers do not contain light modes. The lowest modes of the other towers have the mass $O(m_{\rm KK})$.

We summarize the spectra which we use in this paper. The spectrum of the W tower is given by

$$2S(1; \lambda_{W^{(n)}}) C'(1; \lambda_{W^{(n)}}) + \lambda_{W^{(n)}} \sin^2 \theta_H = 0 . \tag{3.19}$$

which includes the W boson as the lowest mode $W = W^{(0)}$. KK spectrum of the Z tower is given by

$$2S(1;\lambda_{Z^{(n)}})C'(1;\lambda_{Z^{(n)}}) + (1+s_\phi^2)\lambda_{Z^{(n)}}\sin^2\theta_H = 0 \ , \tag{3.20}$$

which includes the Z boson $Z = Z^{(0)}$. We use c_ϕ and s_ϕ which are given by

$$c_\phi = \frac{g_A}{\sqrt{g_A^2+g_B^2}} \ , \quad s_\phi = \frac{g_B}{\sqrt{g_A^2+g_B^2}} \ , \quad \cos\theta_W = \frac{1}{\sqrt{1+s_\phi^2}} \ . \tag{3.21}$$

The spectrum of the photon tower is given by

$$C'(1;\lambda_{\gamma^{(n)}}) = 0 \ , \tag{3.22}$$

which includes a massless photon $\lambda_{\gamma^{(0)}} = 0$. The spectrum of the Z_R tower is given by

$$C(1;\lambda_{Z_R^{(n)}}) = 0 \ , \tag{3.23}$$

$A_z(x,z)$ and $B_z(x,z)$ are expanded in KK towers as

$$\begin{aligned}
\tilde{A}_z(x,z) &= \sum_{a=1}^{3}\hat{G}^a + \sum_{a=1}^{3}\hat{D}^a + \hat{H}, \\
\hat{G}^a &= \sum_n G^{a(n)}(x)\left\{u^L_{G^{(n)}}T^{a_L} + u^R_{G^{(n)}}T^{a_R}\right\}, \\
\hat{D}^a &= \sum_n D^{a(n)}(x)\left\{u^L_{D^{(n)}}T^{a_L} + u^R_{D^{(n)}}T^{a_R} + \hat{u}_{D^{(n)}}T^{\hat{a}}\right\}, \\
\hat{H} &= \sum_n H^{(n)}(x)u_{H^{(n)}}T^{\hat{4}}, \\
B_z(x,z) &= \sum_n B^{(n)}(x)u_{B^{(n)}}T_B \ .
\end{aligned} \tag{3.24}$$

The spectrum of the D tower is given by

$$\begin{aligned}
&S(1;\lambda_{D^{(n)}})C'(1;\lambda_{D^{(n)}}) + \lambda_{D^{(n)}}\sin^2\theta_H \\
&= C(1;\lambda_{D^{(n)}})S'(1;\lambda_{D^{(n)}}) - \lambda_{D^{(n)}}\cos^2\theta_H = 0 \ .
\end{aligned} \tag{3.25}$$

3.2 Fermions and brane interactions in the $SO(5)\times U(1)$ GHU

In this subsection we introduce the five dimensional fermions. In the bulk region there are quark-lepton multiplets Ψ_a which are represented by vector **5** of $SO(5)$. These multiplets contain the four dimensional SM fermions and exotic fermions. On Planck brane at $y = 0$

($z = 1$) we introduce the right-handed brane fermions $\hat{\chi}_{\alpha R}$ and brane scalar $\hat{\Phi}$, which are (**2**,**1**) and (**1**,**2**) representation of $SU(2)_L \times SU(2)_R$, respectively. All exotic fermions acquire masses of $O(m_{\rm KK})$ by brane interactions on the Planck brane. The brane interactions are gauge-invariant under $SO(4) \times U(1)_X \times SU(3)_C$. The scalar $\hat{\Phi}$ on the Planck brane induces couplings among Ψ_a and $\hat{\chi}_{\alpha R}$. With these brane fermions all four-dimensional anomalies in $SO(4) \times U(1)_X$ are cancelled[12]. This anomaly is known as breaking the Ward-Takahashi identity by 1-loop triangle diagrams of axial current coupled to two gauge bosons. In the SM, this anomaly is accidentally cancelled.

Additional fermions Ψ_{F_i} are introduced in the spinor representation **4** of $SO(5)$[7, 10, 12]. This fermions Ψ_{F_i} are needed to obtain minimum $\theta_H \neq \pi/2$ for Higgs effective potential. The effective potentials for vectorial fermions and spinorial fermions have π and 2π periodicity, respectively. We discuss the detail of the effective potential in Sec.4. This fermion is called the $SO(5)$-spinor fermion or the dark fermion. In Sec.6 we study the dark fermions as a candidate of the dark matter.

3.2.1 The fermions in the bulk region

The bulk part of the action is given by

$$
\begin{aligned}
S_{\rm bulk}^{\rm fermion} &= \int d^5x\sqrt{-G}\left[\sum_a \bar{\Psi}_a \mathcal{D}(c_a)\Psi_a + \sum_{i=1}^{n_F} \bar{\Psi}_{F_i}\mathcal{D}(c_{F_i})\Psi_{F_i}\right], \\
\mathcal{D}(c) &= \Gamma^A e_A{}^M\Big(\partial_M + \frac{1}{8}\omega_{MBC}[\Gamma^B,\Gamma^C] \\
&\qquad -ig_A A_M - ig_B Q_X B_M - ig_C Q^{\rm color} G_M)\Big) - c\sigma'(y)\ . \qquad (3.26)
\end{aligned}
$$

$Q^{\rm color} = 1$ for quark-multiplets and $Q^{\rm color} = 0$ otherwise. We introduce n_F kinds of Ψ_{F_i} with bulk mass parameters c_{F_i}. In the simplest case, all Ψ_{F_i} are degenerate, which have the same bulk mass c_F. And we can choose the $U(1)_X$ charge such that Ψ_{F_i} has neutral components.

The electric charge is given by

$$
Q_{\rm EM} = T^{3_L} + T^{3_R} + Q_X\ . \qquad (3.27)
$$

In the fermion part $\bar{\Psi} = i\Psi^\dagger\Gamma^0$ and Γ^M matrices are given by

$$
\Gamma^\mu = \begin{pmatrix} & \sigma^\mu \\ \bar{\sigma}^\mu & \end{pmatrix}\ ,\ \Gamma^5 = \begin{pmatrix} 1 & \\ & -1 \end{pmatrix},\ \sigma^\mu = (1,\ \vec{\sigma})\ ,\ \bar{\sigma}^\mu = (-1,\ \vec{\sigma})\ . \qquad (3.28)
$$

The $c\sigma'(y)$ term in the action (3.26) gives a bulk kink mass. When the dimensionless parameter c changes, profiles of fermion wave function change.

The orbifold boundary conditions at $y_0 = 0$ and $y_1 = L$ are given by

$$\begin{aligned}
&\Psi_a(x, y_j - y) = P_{\rm vec}\Gamma^5\Psi_a(x, y_j + y),\\
&\Psi_{F_i}(x, y_j - y) = \eta_{F_i}(-1)^j P_{\rm sp}\Gamma^5\Psi_{F_i}(x, y_j + y),\\
&P_{\rm sp} = {\rm diag}\,(+1, +1, -1, -1).
\end{aligned} \tag{3.29}$$

$P_{\rm vec}$ is shown at boundary condition (3.8). The dark fermion has no zero mode because of the boundary condition (3.29). The lowest mode of the dark fermions are 1st KK mode. When for small θ_H, with $\eta_{F_i} = +1$ the dark fermions $F_i^{+(n)}, F_i^{0(n)}$ for odd number of KK modes (including the lowest mode) couple to $SU(2)_R$ gauge bosons. On the other hand, the dark fermions $F_i^{+(n)}, F_i^{0(n)}$ for even number of KK mode couple to $SU(2)_L$ gauge bosons mainly. When for small θ_H, with $\eta_{F_i} = -1$ the dark fermions $F_i^{+(n)}, F_i^{0(n)}$ for odd number of KK modes couple to $SU(2)_L$ gauge bosons mainly, whereas the dark fermions $F_i^{+(n)}, F_i^{0(n)}$ for even number of KK mode couple to $SU(2)_R$ gauge bosons.

Quark-lepton multiplets Ψ_a are decomposed into $SO(4)$ vectors and singlets. One $SO(4)$ vector multiplet contains two $SU(2)_L$ doublets. In each generation

$$\begin{aligned}
&\Psi_1 = \left[\begin{pmatrix}T\\B\end{pmatrix}, \begin{pmatrix}t\\b\end{pmatrix}, t'\right]_{2/3}, \quad \Psi_2 = \left[\begin{pmatrix}U\\D\end{pmatrix}, \begin{pmatrix}X\\Y\end{pmatrix}, b'\right]_{-1/3},\\
&\Psi_3 = \left[\begin{pmatrix}\nu_\tau\\\tau\end{pmatrix}, \begin{pmatrix}L_{1X}\\L_{1Y}\end{pmatrix}, \tau'\right]_{-1}, \quad \Psi_4 = \left[\begin{pmatrix}L_{2X}\\L_{2Y}\end{pmatrix}, \begin{pmatrix}L_{3X}\\L_{3Y}\end{pmatrix}, \nu'_\tau\right]_{0},
\end{aligned} \tag{3.30}$$

where the subscripts denote Q_X. These t, b are not 4-dimensional top and bottom quarks but five dimensional field. We take the bulk mass parameters $c_1 = c_2$ and $c_3 = c_4$ in each generation. The Wilson line phase θ_H mixes (B, t) with t' in the $Q_{\rm EM} = 2/3$ sector, and (D, X) with b' in the $Q_{\rm EM} = -1/3$ sector, respectively. Zero modes appear in

$$\begin{aligned}
&\left[Q_{1L} = \begin{pmatrix}T_L\\B_L\end{pmatrix}, q_L = \begin{pmatrix}t_L\\b_L\end{pmatrix}, t'_R\right], \left[Q_{2L} = \begin{pmatrix}U_L\\D_L\end{pmatrix}, Q_{3L} = \begin{pmatrix}X_L\\Y_L\end{pmatrix}, b'_R\right],\\
&\left[\ell_L = \begin{pmatrix}\nu_{\tau L}\\\tau_L\end{pmatrix}, L_{1L} = \begin{pmatrix}L_{1XL}\\L_{1YL}\end{pmatrix}, \tau'_R\right], \left[L_{2L} = \begin{pmatrix}L_{2XL}\\L_{2YL}\end{pmatrix}, L_{3L} = \begin{pmatrix}L_{3XL}\\L_{3YL}\end{pmatrix}, \nu'_{\tau R}\right],
\end{aligned} \tag{3.31}$$

with the boundary condition in (3.29).

3.2.2 The brane interactions

We denote the brane fermions

$$\hat{\chi}^q_{1R} = \begin{pmatrix} \hat{T}_R \\ \hat{B}_R \end{pmatrix}_{7/6}, \quad \hat{\chi}^q_{2R} = \begin{pmatrix} \hat{U}_R \\ \hat{D}_R \end{pmatrix}_{1/6}, \quad \hat{\chi}^q_{3R} = \begin{pmatrix} \hat{X}_R \\ \hat{Y}_R \end{pmatrix}_{-5/6},$$

$$\hat{\chi}^l_{1R} = \begin{pmatrix} \hat{L}_{1XR} \\ \hat{L}_{1YR} \end{pmatrix}_{-3/2}, \quad \hat{\chi}^l_{2R} = \begin{pmatrix} \hat{L}_{2XR} \\ \hat{L}_{2YR} \end{pmatrix}_{1/2}, \quad \hat{\chi}^l_{3R} = \begin{pmatrix} \hat{L}_{3XR} \\ \hat{L}_{3YR} \end{pmatrix}_{-1/2}, \tag{3.32}$$

where the subscripts denote Q_X. $\hat{\chi}^q_{\alpha R}$'s are $SU(3)_C$ triplets. The brane interactions connect B to $\hat{B}_R$, U and t to $\hat{U}_R$, in the $Q_{\rm EM} = 2/3$ sector, whereas they connect D and b to $\hat{D}_R$, and X to $\hat{X}_R$, in the $Q_{\rm EM} = -1/3$ sector.

The brane part of the action is given by

$$\begin{aligned}
S_{\rm brane} = \int d^5x\sqrt{-G}\,\delta(y)\Big\{ & -(D_\mu\hat{\Phi})^\dagger D^\mu\hat{\Phi} - \lambda_{\hat{\Phi}}(\hat{\Phi}^\dagger\hat{\Phi} - w^2)^2 \\
& + \sum_{\alpha=1}^{3}\left(\hat{\chi}^{q\dagger}_{\alpha R}\, i\bar{\sigma}^\mu D_\mu \hat{\chi}^q_{\alpha R} + \hat{\chi}^{l\dagger}_{\alpha R} i\bar{\sigma}^\mu D_\mu \hat{\chi}^l_{\alpha R}\right) \\
& - i\Big[\kappa^q_1 \hat{\chi}^{q\dagger}_{1R}\check{\Psi}_{1L}\tilde{\hat{\Phi}} + \tilde{\kappa}^q \hat{\chi}^{q\dagger}_{2R}\check{\Psi}_{1L}\hat{\Phi} + \kappa^q_2 \hat{\chi}^{q\dagger}_{2R}\check{\Psi}_{2L}\tilde{\hat{\Phi}} + \kappa^q_3 \hat{\chi}^{q\dagger}_{3R}\check{\Psi}_{2L}\hat{\Phi} - ({\rm h.c.})\Big] \\
& - i\Big[\tilde{\kappa}^l \hat{\chi}^{l\dagger}_{3R}\check{\Psi}_{3L}\tilde{\hat{\Phi}} + \kappa^l_1 \hat{\chi}^{l\dagger}_{1R}\check{\Psi}_{3L}\hat{\Phi} + \kappa^l_2 \hat{\chi}^{l\dagger}_{2R}\check{\Psi}_{4L}\tilde{\hat{\Phi}} + \kappa^l_3 \hat{\chi}^{l\dagger}_{3R}\check{\Psi}_{4L}\hat{\Phi} - ({\rm h.c.})\Big]\Big\},
\end{aligned}$$

$$D_\mu\hat{\Phi} = \Big(\partial_\mu - ig_A\sum_{a_R=1}^{3} A^{a_R}_\mu T^{a_R} - iQ_X g_B B_\mu\Big)\hat{\Phi}\,,$$

$$D_\mu\hat{\chi}_{\alpha R} = \Big(\partial_\mu - ig_A\sum_{a_L=1}^{3} A^{a_L}_\mu T^{a_L} - iQ_X g_B B_\mu - ig_C Q^{\rm color} G_\mu\Big)\hat{\chi}_{\alpha R}\,,$$

$$\check{\Psi}_{1L} = \begin{pmatrix} T_L & t_L \\ B_L & b_L \end{pmatrix} \quad \text{etc.}, \quad \tilde{\hat{\Phi}} = i\sigma_2\hat{\Phi}^*\,. \tag{3.33}$$

The vacuum expectation value of the brane scalar $\langle\hat{\Phi}\rangle = (0, w)^t \neq 0$ breaks $SU(2)_R\times U(1)_X$ to $U(1)_Y$. The brane mass term is given by

$$\begin{aligned}
S^{\rm mass}_{\rm brane} = \int d^5x\sqrt{-G}\,\delta(y)\Big\{ & -\sum_{\alpha=1}^{3} i\mu^q_\alpha(\hat{\chi}^{q\dagger}_{\alpha R}Q_{\alpha L} - Q^\dagger_{\alpha L}\hat{\chi}^q_{\alpha R}) - i\tilde{\mu}^q(\hat{\chi}^{q\dagger}_{2R}q_L - q^\dagger_L\hat{\chi}^q_{2R}) \\
& - \sum_{\alpha=1}^{3} i\mu^l_\alpha(\hat{\chi}^{l\dagger}_{\alpha R}L_{\alpha L} - L^\dagger_{\alpha L}\hat{\chi}^l_{\alpha R}) - i\tilde{\mu}^l(\hat{\chi}^{l\dagger}_{3R}\ell_L - \ell^\dagger_L\hat{\chi}^l_{3R})\Big\},
\end{aligned}$$

$$\frac{\mu^q_\alpha}{\kappa^q_\alpha} = \frac{\tilde{\mu}^l}{\tilde{\kappa}^q} = \frac{\mu^l_\alpha}{\kappa^l_\alpha} = \frac{\tilde{\mu}^l}{\tilde{\kappa}^l} = w\,, \tag{3.34}$$

where $\mu_\alpha, \tilde{\mu}$ are brane mass parameters. In this paper we do not consider off-diagonal parts of the brane interactions in the generation of quarks and leptons. In general, couplings of brane interactions, κs in (3.33), can be matrices in generations, which induces CKM and MNS matrices. All of $\mu_\alpha, \tilde{\mu}$ and w can be taken to be real and positive. In the case of $\mu_\alpha, \tilde{\mu} \gg m_{\rm KK}$, only $\tilde{\mu}^q/\mu_2^q$ and $\tilde{\mu}^l/\mu_3^l$ become relevant at low energies.

3.2.3 The wave functions and the mass function of the fermions

The fermions with a bulk mass parameter c are expanded by the terms of Bessel functions,

$$\begin{aligned}
\begin{pmatrix} C_L \\ S_L \end{pmatrix}(z;\lambda,c) &= \pm\frac{\pi}{2}\lambda\sqrt{zz_L}F_{c+\frac{1}{2},c\mp\frac{1}{2}}(\lambda z,\lambda z_L)\ , \\
\begin{pmatrix} C_R \\ S_R \end{pmatrix}(z;\lambda,c) &= \mp\frac{\pi}{2}\lambda\sqrt{zz_L}F_{c-\frac{1}{2},c\pm\frac{1}{2}}(\lambda z,\lambda z_L)\ .
\end{aligned} \tag{3.35}$$

They satisfy

$$\begin{aligned}
&D_+(c)\begin{pmatrix} C_L \\ S_L \end{pmatrix} = \lambda\begin{pmatrix} S_R \\ C_R \end{pmatrix},\quad D_-(c)\begin{pmatrix} C_R \\ S_R \end{pmatrix} = \lambda\begin{pmatrix} S_L \\ C_L \end{pmatrix}, \\
&D_\pm(c) = \pm\frac{d}{dz} + \frac{c}{z}\ ,
\end{aligned} \tag{3.36}$$

and

$$\begin{aligned}
&C_R = C_L = 1\ ,\quad S_R = S_L = 0 \quad \text{for } z = z_L\ , \\
&C_LC_R - S_LS_R = 1\ ,\quad S_L(z;\lambda,-c) = -S_R(z;\lambda,c)\ .
\end{aligned} \tag{3.37}$$

The left-handed fermions are expanded by $C_L(z;\lambda,c)$ or $S_L(z;\lambda,c)$. The right-handed fermions are expanded by $C_R(z;\lambda,c)$ or $S_R(z;\lambda,c)$. The wave function of the left-handed fermions are localized at the Planck brane with larger bulk mass parameter c, whareas The wave function of the right-handed fermions are localized at the TeV brane with larger bulk mass parameter c.

We summarize the mass functions of up-type quarks (top), down-type quarks (bottom) and the dark fermions. The mass spectrum of the KK tower of the up-type quark are given by

$$2\left\{1+\left(\frac{\mu_2^q}{\tilde{\mu}^q}\right)^2\right\}S_L(1;\lambda_{t^{(n)}},c_t)S_R(1;\lambda_{t^{(n)}},c_t) + \left(\frac{\mu_2^q}{\tilde{\mu}^q}\right)^2\sin^2\theta_H = 0\ . \tag{3.38}$$

The mass of the KK tower of the up-type quark is given by $m_{t^{(n)}} = \lambda_{t^{(n)}} k$. The ratio $\mu_2^q/\tilde{\mu}^q$ in (3.38) is determined by mass ratio of a/a. The mass spectrum of the down-type quark are given by

$$2\left\{1 + \left(\frac{\mu_2^q}{\tilde{\mu}^q}\right)^2\right\} S_L(1; \lambda_{b^{(n)}}, c_t) S_R(1; \lambda_{b^{(n)}}, c_t) + \sin^2\theta_H = 0. \tag{3.39}$$

The mass of the up-type quark is given by $m_{b^{(n)}} = \lambda_{b^{(n)}} k$. For a lepton mupltiplet (ν_τ, τ), the wave functions are given by the following replacement rules,

$$\begin{pmatrix} U \\ B \\ t \\ t' \end{pmatrix} \to \begin{pmatrix} \nu_\tau \\ L_{2Y} \\ L_{3X} \\ \nu'_\tau \end{pmatrix}, \quad \begin{pmatrix} b \\ D \\ X \\ b' \end{pmatrix} \to \begin{pmatrix} L_{3Y} \\ \tau \\ L_{1Y} \\ \tau' \end{pmatrix},$$

$$(\tilde{\mu}^q, \mu_2^q) \to (\mu_3^\ell, \tilde{\mu}^\ell) \ , \quad (\mu_3^q, \mu_1^q) \to (\mu_1^\ell, \mu_2^\ell) \ ,$$

$$(c_1, c_2) \to (c_4, c_3) \ . \tag{3.40}$$

The mass spectrum of the KK tower of the dark fermion Ψ_{F_i} are given by

$$C_L(1; \lambda_{i,n}, c_{F_i}) C_R(1; \lambda_{i,n}, c_{F_i}) - \sin^2\frac{\theta_H}{2} = 0 \ . \tag{3.41}$$

The mass of the KK tower of the dark fermions is given by $m_{F_i^{(n)}} = \lambda_{i,n} k$. We determine the bulk mass parameters c in the next section 4.

4 The effective potential and the universality

We generate Higgs effective potential and we show the minimum of effective potential is controlled by gauge fields, top quark multiplet and dark fermions. We find the universal relation which is independent on the detail of the dark fermion sector. The universality relations appear among θ_H, the KK mass $m_{\rm KK}$, the masses of $Z^{(1)}$ and $\gamma^{(1)}$, and the Higgs self-couplings[7].

4.1 $V_{\rm eff}(\theta_H)$ and observed Higgs boson

4.1.1 Relevant parameters

Firstly we consider relevant parameters in this model. We have two parameters z_L and k (or L) from Randall-Sundrum warped spacetime in (3.1). Gauge couplings g_A and g_B come from $SO(5)_L \times U(1)_X$ gauge symmetry. We interpret the gauge couplings as the angles

s_ϕ and c_ϕ in (3.21). Top and bottom mass spectrums in (3.38) and (3.39) are determined by c_t and $\tilde{\mu}^q/\mu_2^q$. The detail of the degenerate dark fermions is determined by n_F and c_F in (3.26) and (3.41). In the non-degenerate case, we need n_{F_i} and c_{F_i} for each dark fermions Ψ_{F_i}. These eight parameters k, z_L, g_A, g_B, c_t, $\tilde{\mu}/\mu_2$, c_F and n_F are relevant. Other brane mass parameters are irrelevant as $\mu_\alpha, \tilde{\mu}, w \gg m_{\rm KK}$. When these parameters are determined, $V_{\rm eff}(\theta_H)$ is determined. We use the six observed values, m_Z, α_w, $\sin^2\theta_W$, m_t, m_b, and m_H[16]. We treat z_L and n_F as free parameters.

Global minimum θ_H and Higgs mass m_H are determined after determining the effective potential. The effective potential is determined by the details of the particles. The details of the particles are determined by the global minimum θ_H. Therefore all parameters must be determined self-consistently.

4.1.2 Effective potential without dark fermions

Let us first consider no dark fermions ($SO(5)$-spinor fermions) Ψ_{F_i} case. In the effective potentials, the contributions from the gauge bosons and top quark multiplet are positive and negative, respectively. The contributions of other quarks and leptons are smaller than the top quark multiplet and negligible. Because the contribution of the top quark mulitplet is larger than the contributions of gauge bosons, the total effective potential is shown in left panel of Fig. 4. This potential has π periodicity. This minimum of the effective potential is always located at $\theta_H = \pi/2$. In this theory all 3-point Higgs couplings of quarks, leptons and W and Z bosons vanish because these 3-point Higgs couplings are proportional to $\cos\theta_H$. Therefore this Higgs boson becomes stable. In 2012 the Higgs boson has been discovered by LHC experiments. The existence of the unstable Higgs boson indicates that there must be additional fields which gives rise to contributions of different periodicity, say 2π. This is fulfilled by the dark fermions. This fermion has 2π periodicity in right panel of Fig. 4. The sum of both contributions generate the minimum $\theta_H \neq \pi/2$. The larger dark fermions contribute, the smaller Wilson line phase θ_H is. In this way we control the place of minimum.

4.1.3 Effective potential with degenerate dark fermions

We determine the relevant parameters and the effective potential. Firstly we calculate the case of $(z_L, n_F) = (10^5, 5)$ as an example. As we mentioned we should determine the parameters self-consistently. Firstly we fix $\theta_1 = 0.120$ tentatively. The minimum of $V_{\rm eff}(\theta_H)$

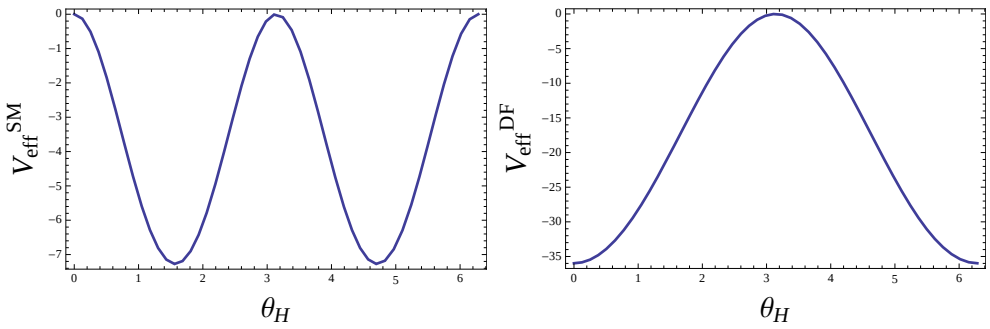

Figure 4: Left figure is effective potential for contributions of gauge bosons and fermions with vectorial representation. Right figure is effective potential for contributions of fermions with spinorial representation (dark fermions).

is located at θ_1. In general we cannot get $m_H = 126$ GeV from this minimum. If we do not obtain the 126 GeV Higgs mass, we change the value θ_1.

We determine k from Z boson mass sepctrum (3.20),

$$F_k(x = \frac{z_L}{k}, \theta_1, m_{Z^{(0)}}) = 2S(1; m_{Z^{(0)}}x)C'(1; m_{Z^{(0)}}x) + \frac{m_{Z^{(0)}}x}{1+s_\phi^2}\sin^2\theta_1, \tag{4.1}$$

where the angle s_ϕ is given by Weinberg angle $\sin^2\theta_W = 0.231$. The mass eigenvalue $\lambda_{Z^{(0)}}$ is given by m_Z/k. We use $m_Z = 91.19$ GeV. In Fig. 5 z_L/k is 4.17×10^{-1}/TeV. We determine $k = 2.27 \times 10^5$ TeV from $F_k(x, \theta_1, m_{Z^{(0)}}) = 0$. At this time we can determine $L = (\text{Log } z_L)/k = 5.08 \times 10^{-5}$/TeV and KK mass $m_{\rm KK} = \pi k/(z_L - 1) = 7.12$ TeV.

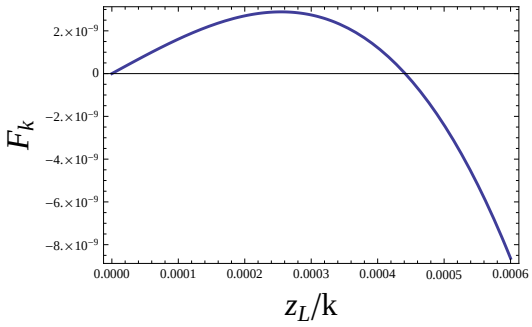

Figure 5: In the case of $(z_L, n_F) = (10^5, 5)$ and $\theta_1 = 0.120$, we plot (4.1). Horizontal line x is z_L/k. Solution of z_L/k is 4.17×10^{-1}/TeV. We obtain $k = 2.27 \times 10^5$ TeV.

Next, we determine c_t from spectra of top and bottom quark towers (3.38) and (3.39). We sum (3.38) and (3.39),

$$F_t(c_t, \theta_1) = S_L(1; \lambda_{t^{(n)}}, c_t)S_R(1; \lambda_{t^{(n)}}, c_t) + S_L(1; \lambda_{b^{(n)}}, c_t)S_R(1; \lambda_{b^{(n)}}, c_t) + \frac{1}{2}\sin^2\theta_H \ , \tag{4.2}$$

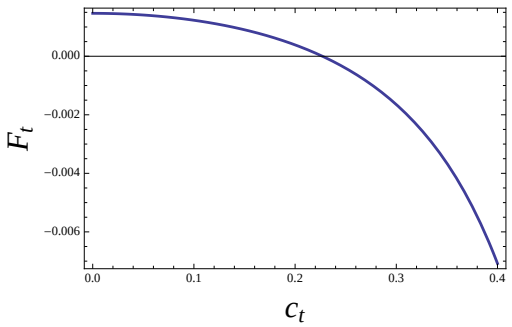

Figure 6: In the case of $(z_L, n_F) = (10^5, 5)$ and $\theta_1 = 0.120$, we plot (4.2). Horizontal line is c_t. we determine $c_t = 0.227$.

where we take $c_t = c_b$. We use the observed values $m_t = k\lambda_{t^{(1)}} = 171.17$ GeV and $m_b = k\lambda_{b^{(1)}} = 2.89$ GeV. From (4.2) we determine $c_t = 0.227$ in Fig.6. We can also determine $|\tilde{\mu}^q/\mu_2^q| = m_b/m_t$ [10].

We calculate the effective potential (4.10) with a parameter c_F. The effective potential is given by

$$\begin{aligned} V_{\text{eff}} &= \frac{1}{(4\pi)^2}\int_0^\infty dy\, y^3 \ln\, \rho(iy) \\ &= \frac{\left(kz_L^{-1}\right)^4}{(4\pi)^2}\int_0^\infty dq\, q^3 \ln\, \rho(iq), \end{aligned} \tag{4.3}$$

where y is not coordinate of the extra dimension. Second line is $y = kq/z_L$. ρ is the mass spectrum function. This formula is shown in Appendix C. In this effective potential (4.3), we ignore the positive sign for bosons and the negative sign for fermions. The 1-loop effective potential V_{eff} has the contributions from only the KK towers whose mass spectra depend on θ_H. Because in (4.3) the argument of mass spectrums is imaginary, we transform modified Bessel functions from Bessel functions in the mass spectra. Modified Bessel functions are given by

$$\begin{aligned} I_\alpha(x) = i^{-\alpha}J(ix), \quad K_\alpha(x) = \tfrac{\pi}{2}i^{\alpha+1}H_\alpha(ix), \\ H_\alpha(x) = J_\alpha(x) + iY_\alpha(x). \end{aligned} \tag{4.4}$$

We transform the mass spectrum (3.19) as an example,

$$\begin{aligned} Q_W &= 1 + \frac{\lambda_{W^{(n)}}\sin^2\theta_H}{2S(1;\lambda_{W^{(n)}})C'(1;\lambda_{W^{(n)}})} \\ &= 1 + \frac{\lambda_{W^{(n)}}\sin^2\theta_H}{-2\frac{\pi}{2}\lambda_{W^{(n)}}F_{1,1}(\lambda_{W^{(n)}},\lambda_{W^{(n)}}z_L)\cdot\frac{\pi}{2}\lambda_{W^{(n)}}^2 z_L F_{0,0}(\lambda_{W^{(n)}},\lambda_{W^{(n)}}z_L)}. \end{aligned}$$

We denote $\lambda_{W^{(n)}} = q/z_L$,

$$Q_W = 1 + \frac{z_L \sin^2\theta_H}{-\frac{\pi^2}{2} q^2 F_{1,1}(q, qz_L) F_{0,0}(q, qz_L)}. \tag{4.5}$$

We transform the Bessel functions in $F_{1,1}(q, qz_L)$ and $F_{0,0}(q, qz_L)$.

$$\begin{aligned} F_{1,1}(qz_L^{-1}, q) &= \frac{2}{\pi} i^{-1} \left\{ I_1(qz_L^{-1}) K_1(q) - K_1(qz_L^{-1}) I_1(q) \right\} , \\ F_{0,0}(qz_L^{-1}, q) &= \frac{2}{\pi} i^{-1} \left\{ I_0(qz_L^{-1}) K_0(q) - K_0(qz_L^{-1}) I_0(q) \right\} . \end{aligned}$$

We define $\hat{F}_{\alpha,\beta}(u, v)$,

$$\hat{F}_{\alpha,\beta}(u, v) = I_\alpha(u) K_\beta(v) - e^{-i(\alpha-\beta)\pi} K_\alpha(u) I_\beta(v) . \tag{4.6}$$

By using (4.6) we obtain

$$\begin{aligned} Q_W &= 1 + \frac{1}{2} \frac{z_L}{q^2 \hat{F}_{1,1}(qz_L^{-1}, q) \hat{F}_{0,0}(qz_L^{-1}, q)} \sin^2\theta_H \\ &= 1 + \frac{1}{2} Q_0[q; \tfrac{1}{2}] \sin^2\theta_H, \end{aligned} \tag{4.7}$$

where

$$Q_0[q; c] = \frac{z_L}{q^2 \hat{F}_{c-\frac{1}{2}, c-\frac{1}{2}}(qz_L^{-1}, q) \hat{F}_{c+\frac{1}{2}, c+\frac{1}{2}}(qz_L^{-1}, q)}. \tag{4.8}$$

By the same way we obtain Q of Z tower, D tower, top tower, bottom tower and dark fermion tower,

$$\begin{aligned} Q_W &= \cos^2\theta_W Q_Z = \frac{1}{2} Q_D = \frac{1}{2} Q_0[q; \frac{1}{2}] \sin^2\theta_H , \\ Q_{\rm top} &= \frac{Q_{\rm bottom}}{r_t} = \frac{Q_0[q; c_t]}{2(1 + r_t)} \sin^2\theta_H , \\ Q_F &= Q_0[q; c_F] \cos^2 \frac{1}{2}\theta_H , \end{aligned} \tag{4.9}$$

where $r_t = (\tilde{\mu}/\mu_2)^2$. Finally we obtain the effective potential from (4.3),

$$\begin{aligned} V_{\rm eff}(\theta_H, c_t, r_t, c_F, n_F, k, z_L, \theta_W; \xi) &= 2(3 - \xi^2) I[Q_W] + (3 - \xi^2) I[Q_Z] + 3\xi^2 I[Q_D] \\ &\quad - 12\{I[Q_{\rm top}] + I[Q_{\rm bottom}]\} - 8 n_F I[Q_F] , \\ I[Q(q; \theta_H)] &= \frac{(kz_L^{-1})^4}{(4\pi)^2} \int_0^\infty dq\, q^3 \ln\{1 + Q(q; \theta_H)\} . \end{aligned} \tag{4.10}$$

In the following we take the 't Hooft–Feynman gauge $\xi = 1$. Coefficients of $I[Q]$ come from degree of freedom of the W, Z, D, top, bottom and dark fermions.

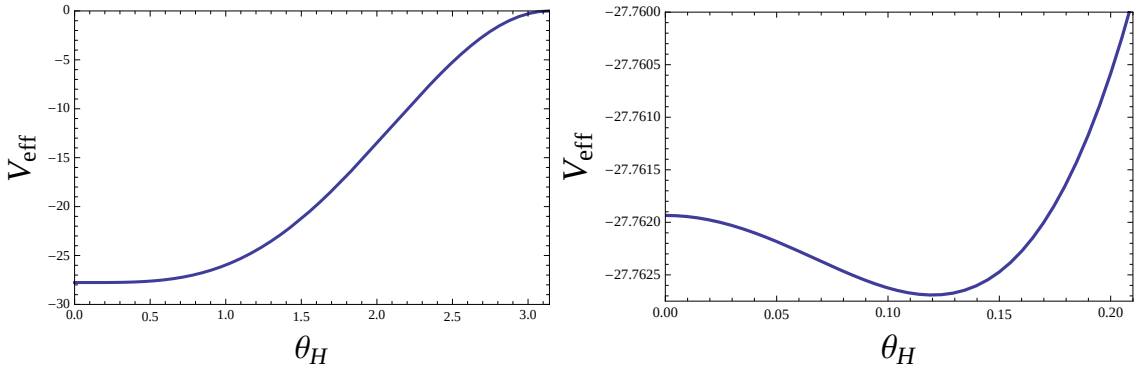

Figure 7: We plot $V_{\rm eff}(\theta_1)$ for $(z_L, n_F) = (10^5, 5)$, $\theta_1 = 0.120$ and $\xi = 1$. In left panel, plot range is from 0 to π. In right panel, plot range is from 0 to 0.2. Global minimum is $\theta_1 = 0.120$. In this case Higgs mass is $m_H = 125$ GeV.

We determine dark fermion mass parameter c_F from the following condition,

$$\left.\frac{dV_{\rm eff}}{d\theta_H}\right|_{\theta_1} = 0. \tag{4.11}$$

The minimum of $V_{\rm eff}(\theta_H)$ is located at θ_1. In the case of $(z_L, n_F) = (10^5, 5)$ and $\theta_1 = 0.120$ we obtain $c_F = 0.382$. Fig. 7 is effective potential for this case.

We evaluate the Higgs mass,

$$m_H^2 = \frac{1}{f_H^2}\left.\frac{d^2V_{\rm eff}}{d\theta_H^2}\right|_{\rm min}, \tag{4.12}$$

where f_H is defined in (3.10). Four dimensional coupling is given by $g_4^2 = 4\pi\alpha/\sin^2\theta_W = 0.652$ where $\alpha = 1/128$. In the case of $\theta_1 = 0.120$ we obtain Higgs mass $m_H = 125$ GeV. Because we want to obtain the Higgs mass $m_H = 126$ GeV, we change θ_H. If the obtained Higgs mass is smaller (larger) than the 126 GeV, we change the smaller (larger) value of θ_1. To reiterate this procedure we can obtain the parameter set for $m_H = 126$ GeV. In the case of $(z_L, n_F) = (10^5, 5)$, we obtain the parameter set, $\theta_H = 0.114$, $k = 2.38 \times 10^5$ TeV, $L = 4.83 \times 10^{-5}$/TeV, $m_{\rm KK} = 7.49$ TeV, $c_t = 0.227$ and $c_F = 0.382$.

When we get $m_H = 126$ GeV, global minimum θ_H is determine and all other quantities such as the mass spectra of all KK towers, gauge couplings of all particles, and Yukawa couplings of all fermions are determined. We calculate the first KK Z boson mass as an example. We use (4.1),

$$F_k(\frac{z_L}{k}, \theta_H, M) = 2S(1; M\frac{z_L}{k})C'(1; M\frac{z_L}{k}) + \frac{M\frac{z_L}{k}}{1+s_\phi^2}\sin^2\theta_H$$

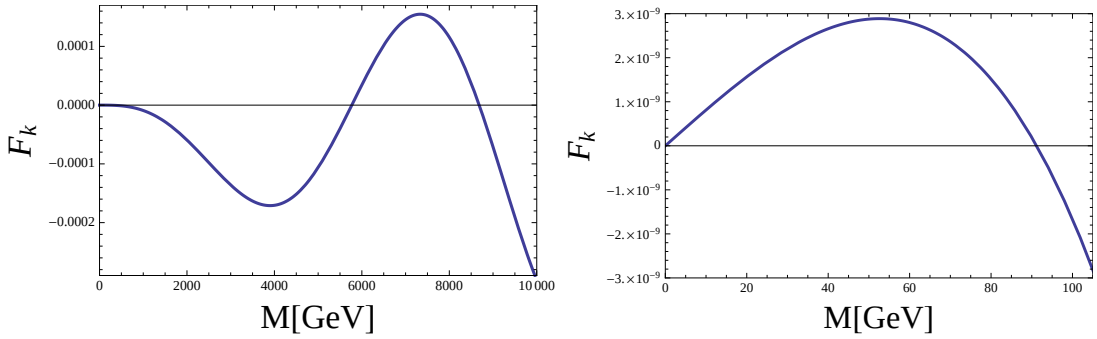

Figure 8: We plot $F_k(k/z_L, \theta_1, m)$ for $(z_L, n_F) = (10^5, 5)$, $\theta_1 = 0.114$ and $\xi = 1$. In left panel, plot range is from 0 to 10^5 GeV. In right panel, plot range is from 0 to 10^2 GeV. The first KK Z boson mass $m_{Z^{(1)}} = 6.07$ TeV. The right panel shows that Z boson mass is 91.2 GeV.

where a variable is m. In left panel of Fig.8 we obtain the first KK Z boson mass $m_{Z^{(1)}} = 6.07$ TeV from $F_k(\frac{z_L}{k}, \theta_H, M) = 0$. The right panel shows that Z boson mass is 91.2 GeV.

We note that in the case of $n_F = 1, 2$ and 3, small z_L cannot reproduce $m_H = 126$ GeV because the small z_L gives $m_H < 126$ GeV. At $c_F = 0$ the lowest mode of dark fermion tower has the largest mass. In the case of $n_F = 1$ and $n_F = 3$ the smallest warp factor is $z_L = 1.66 \times 10^9$ and $z_L = 2.0 \times 10^2$ in Fig. 1 and Fig. 2, respectively. In the case of $n_F \geq 4$ and $z_L < 10^4$, this case cannot reproduce the top mass. At $c_t = 0$ the lowest mode of top quark tower has the largest mass. If the mass of the lowest mode is below the observed top mass at $c_t = 0$ we cannot obtain the top mass.

Determined values for θ_H, $m_{\rm KK}$, $m_{Z^{(1)}}$, etc. are tabulated in Table 2 and 3 in the case of $n_F = 3$ and $n_F = 5$, respectively. The smaller z_L is, the smaller θ_H. The smaller z_L is, the larger $m_{\rm KK}$ is. The small bulk mass parameters c_F and c_t give the large mass m_F and m_t and large contribution to the effective potential. The masses of $Z_R^{(1)}$, $Z^{(1)}$ and $\gamma^{(1)}$ are about $0.8\times m_{\rm KK}$. Dark fermion mass m_F is below the half of the $Z_R^{(1)}$ mass. For large n_F the dark fermion mass m_F (c_F) is smaller (larger) than that for small n_F with the fixed Higgs mass. The mass $m_{F^{(1)}}$ is plotted in Fig. 9 for various n_F. As we mentioned, when $n_F \geq 4$, one cannot reproduce the top quark mass for $z_L < 10^4$. This constraint of top quark mass is severe due to the independence of constructing the effective potential. Therefore we cannot consider the dark fermions mass is too heavy in this calculation. For the small θ_H (large $m_K K$), heavy KK particles are decoupled. We can regard $z_L \to 1$ (flat limit) or $\theta_H \to 0$ as the SM limit. Strictly speaking, we cannot take the SM limit numerically as small z_L cannot reproduce m_t or $m_H = 126$ GeV. If we take this limit actually, we need many dark

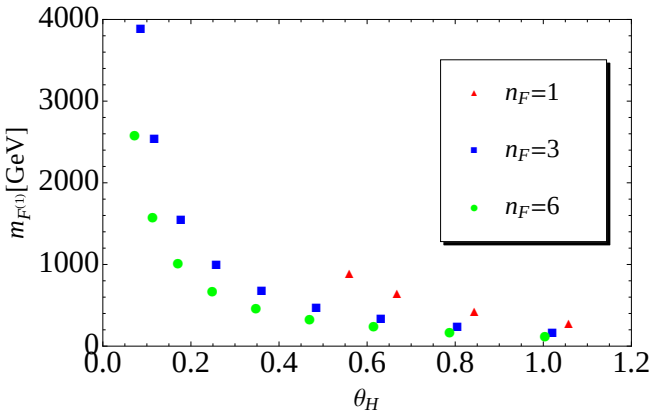

Figure 9: θ_H vs m_F for $m_H = 126\,\mathrm{GeV}$ with n_F degenerate dark fermions. This figure is originally shown in [13].

Table 1: Parameters and masses in the case of degenerate dark fermions with $n_F = 1$. All masses and k are given in units of TeV.

z_L	θ_H	m_{KK}	k	c_t	c_F
10^{12}	1.06	1.51	4.79×10^{11}	0.413	0.395
10^{11}	0.843	1.68	5.36×10^{10}	0.403	0.319
10^{10}	0.668	1.94	6.17×10^{9}	0.391	0.215
1.66×10^{9}	0.548	2.21	1.17×10^{9}	0.380	0.000796

fermions. In the large n_F case the dark fermion mass is too small so that dark fermions appear at low energy. Furthermore gauge symmetry is unbroken at $\theta_H = 0$.

4.1.4 Effective potential with non-degenerate dark fermions

We consider the more general situations. We can introduce n_F kinds of the dark fermions which have different bulk mass parameters. Here we introduce two kinds of the dark fermions. The n_F^h dark fermions have smaller bulk mass parameter c_F^h and heavier mass m_{F_h}, the n_F^l dark fermions have larger bulk mass parameter c_F^l and lighter mass m_{F_l}. The dark fermion part of the effective potential (4.10) change,

$$V_{\mathrm{eff}}^{DF}(\theta_H, c_{F_h}, c_{F_l}, n_{F_h}, n_{F_l}, k, z_L, \theta_W) = -8n_{F_1} I[Q_{F_1}] - 8n_{F_2} I[Q_{F_2}] \ . \tag{4.13}$$

We fix the difference of the bulk mass parameters and determine the c_Fs from the condition (4.11). When $n_F = n_F^h + n_F^l = 5$, a difference $c_F^l - c_F^h = 0.01(0.03)$ leads to $m_{F_h} - m_{F_l} =$ 30 to 80 GeV (80 to 240 GeV). The dark fermion masses $m_{F_h^{(1)}}$ and $m_{F_l^{(1)}}$ in the case of

Table 2: Parameters and masses in the case of degenerate dark fermions with $n_F = 3$. All masses and k are given in units of TeV. This table is originally shown in [7].

z_L	θ_H	$m_{\rm KK}$	k	c_t	c_F	$m_{F^{(1)}}$
10^9	0.485	2.45	7.79×10^8	0.376	0.411	0.465
10^8	0.360	3.05	9.72×10^7	0.357	0.385	0.668
10^7	0.258	3.95	1.26×10^7	0.330	0.353	0.993
10^6	0.177	5.30	1.69×10^6	0.296	0.309	1.54
10^5	0.117	7.29	2.32×10^5	0.227	0.235	2.53
2×10^4	0.086	9.21	5.87×10^4	0.137	0.127	3.88

Table 3: Parameters and masses in the case of degenerate dark fermions with $n_F = 5$. All masses and k are given in units of TeV. This table is originally shown in [13].

z_L	θ_H	$m_{\rm KK}$	k	c_t	c_F	$m_{F^{(1)}}$	$m_{Z_R^{(1)}}$	$m_{Z^{(1)}}$	$m_{\gamma^{(1)}}$
10^9	0.473	2.50	7.97×10^8	0.376	0.459	0.353	1.92	1.97	1.98
10^8	0.351	3.13	9.97×10^7	0.357	0.445	0.502	2.40	2.48	2.48
10^7	0.251	4.06	1.29×10^7	0.330	0.430	0.735	3.11	3.24	3.24
10^6	0.172	5.45	1.74×10^6	0.292	0.410	1.11	4.17	4.37	4.38
10^5	0.114	7.49	2.38×10^5	0.227	0.382	1.75	5.73	6.07	6.08
10^4	0.0730	10.5	3.33×10^4	0.0366	0.333	2.91	8.00	8.61	8.61

$(n_F^h, n_F^l) = (3, 2)$ and $c_F^l - c_F^h = 0.03$ are tabulated in Table 4. For the case of $(n_F^h, n_F^l) = (3, 1)$ a difference $c_F^l - c_F^h = 0.04(0.06)$ leads to $m_{F_h} - m_{F_l} \sim 300$ GeV (400 GeV), which is tabulated in Table 12 in Sec. 6. We tabulate the parameters which is various (n_F^h, n_F^l) with $n_F = 6$ and $c_F^l - c_F^h = 0.06$, Table 5. We also tabulate the parameters which is various $c_F^l - c_F^h$ with $n_F = 5$, Table 6. As increase the number of the light dark fermions n_F^l, masses of both heavy and light dark fermions become heavy. One finds that in Fig.5 the mass difference of the dark fermions almost unaffects the effective potential $V_{\rm eft}(\theta_H)$. We find that global minimum θ_H is numerically unchanged to the accuracy of three digits by this mass difference. Therefore we do not need to consider changing the numerical values of $m_{\rm KK}$, k, c_t, $m_{Z_R^{(1)}}$, $m_{Z^{(1)}}$, and $m_{\gamma^{(1)}}$ when the dark fermions are non-degenerate.

We have constraints for parameter sets by experiments at this time. The low energy data, the S parameter constraint, and the tree-level unitarity constraint indicate small $\theta_H < 0.3$[8][17]. The KK mass scale $m_{\rm KK}$ is predicted to be $3 \sim 7$ TeV for $\theta_H = 0.1 \sim 0.3$. If the dark fermion is charged and long-lived particle, its current limit is $m_{F^{(1)}} > 0.5$ TeV [18][19]. In Sec.6, however, we consider charged components of the dark fermion decay sufficiently fast. In this case, this current limit cannot be applied for our dark fermions.

Table 4: Parameters and masses in the case of non-degenerate dark fermions with $(n_F^h, n_F^l) = (3, 2)$ and $c_F^l - c_F^h = 0.03$. Masses are given in units of TeV. The values of $m_{\rm KK}$, k, c_t, $m_{Z^{(1)}}$, $m_{Z_R^{(1)}}$, and $m_{\gamma^{(1)}}$ are the same in three digits as those in Table 3 in the degenerate case.

z_L	θ_H	c_F^h	$m_{F_h^{(1)}}$	$m_{F_l^{(1)}}$
10^9	0.473	0.447	0.384	0.304
10^8	0.351	0.434	0.540	0.444
10^7	0.251	0.418	0.781	0.663
10^6	0.172	0.398	1.17	1.02
10^5	0.114	0.370	1.83	1.64
10^4	0.0730	0.321	3.01	2.77

Table 5: Parameters and masses in the case of non-degenerate dark fermions with $n_F = 6$, $c_F^l - c_F^h = 0.06$. Masses are given in units of TeV.

(n_F^h, n_F^l)	z_L	θ_H	$m_{\rm KK}$	k	c_t	c_F^h	$m_{F_h^{(1)}}$	$m_{F_l^{(1)}}$
(6,0)	10^5	0.113	7.56	2.41×10^5	0.227	0.414	1.57	
	10^4	0.0724	10.5	3.36×10^4	0.0365	0.379	2.57	
(5,1)	10^5	0.113	7.56	2.41×10^5	0.227	0.404	1.63	1.25
	10^4	0.0724	10.5	3.36×10^4	0.0365	0.369	2.65	2.17
(4,2)	10^5	0.113	7.56	2.41×10^5	0.227	0.394	1.69	1.31
	10^4	0.0724	10.5	3.36×10^4	0.0365	0.359	2.73	2.25
(3,3)	10^5	0.113	7.56	2.41×10^5	0.227	0.384	1.76	1.38
	10^4	0.0724	10.5	3.36×10^4	0.0365	0.349	2.81	2.33
(2,4)	10^5	0.113	7.56	2.41×10^5	0.227	0.374	1.82	1.44
	10^4	0.0724	10.5	3.36×10^4	0.0365	0.339	2.89	2.41
(1,5)	10^5	0.113	7.56	2.41×10^5	0.227	0.364	1.88	1.50
	10^4	0.0724	10.5	3.36×10^4	0.0365	0.329	2.967	2.49

Table 6: Parameters and masses in the case of non-degenerate dark fermions with $n_F = 5$, $z_L = 10^4$ and various $c_F^l - c_F^h$. In this case, parameters are $(\theta_H, m_{\rm KK}, k, c_t) = (0.073, 10.5\ \text{TeV}, 3.33 \times 10^4\ \text{TeV}, 0.0366)$. Masses are given in units of TeV.

$c_F^l - c_F^h$	(n_F^h, n_F^l)	c_F^h	$m_{F_h^{(1)}}$	$m_{F_l^{(1)}}$
0	(5,0)	0.333	2.91	
0.01	(4,1)	0.331	2.93	2.85
	(3,2)	0.329	2.94	2.87
	(2,3)	0.327	2.96	2.88
	(1,4)	0.325	2.97	2.90
0.02	(4,1)	0.329	2.94	2.79
	(3,2)	0.325	2.97	2.82
	(2,3)	0.321	3.01	2.85
	(1,4)	0.317	3.04	2.88
0.03	(4,1)	0.327	2.96	2.72
	(3,2)	0.321	3.01	2.77
	(2,3)	0.315	3.05	2.82
	(1,4)	0.309	3.10	2.87
0.04	(4,1)	0.325	2.98	2.66
	(3,2)	0.317	3.04	2.73
	(2,3)	0.309	3.10	2.79
	(1,4)	0.301	3.16	2.85
0.05	(4,1)	0.323	2.99	2.60
	(3,2)	0.313	3.07	2.68
	(2,3)	0.303	3.15	2.76
	(1,4)	0.293	3.22	2.84
0.06	(4,1)	0.321	3.01	2.54
	(3,2)	0.309	3.10	2.63
	(2,3)	0.297	3.20	2.73
	(1,4)	0.285	3.29	2.82

4.2 The universality

In previous subsection we determined parameter sets k, g_A, g_B, c_t, $\tilde{\mu}/\mu_2$ and c_F from m_Z, α_w, $\sin^2\theta_W$, m_t, m_b, and m_H. Free parameters are z_L and n_F. We can determine parameters, $m_{\rm KK}$, the mass spectra, Higgs cubic and quartic self-couplings λ_3, λ_4 and Yukawa couplings, when we fix the warp factor z_L and the number of the dark fermions n_F. We plot $m_{\rm KK}$, $Z_R^{(1)}$ mass, $Z^{(1)}$ mass, $\gamma^{(1)}$ mass, first KK top $t^{(1)}$ mass, couplings $Z^{(1)}\bar{q}q$, λ_3 and λ_4 against θ_H for the various n_F, Fig.10–15. The formula for couplings of $Z^{(n)}\bar{q}q$ are shown in Appendix A. In the case of $n_F = 0$, a parameters set for $m_H = 126$ GeV is $z_L = 1.5 \times 10^{13}$, $\theta_H = \pi/2$, $c_t = 0.422$ and $k = 6.55 \times 10^{12}$ TeV. In the case of $n_F = 0$ a parameter set for $m_H = 125$ GeV is $z_L = 10^{13}$, $\theta_H = \pi/2$, $c_t = 0.421$ $k = 4.34 \times 10^{12}$ TeV. In Fig.10–15, one finds that all plots are on the same curves. In Fig.10 and Fig.11, the blue curves are the fitting curves. These fitting curves for $m_{\rm KK}$, $Z_R^{(1)}$, $Z^{(1)}$, $\gamma^{(1)}$ and $m_{t^{1)}}$ masses are given by,

$$
\begin{aligned}
&m_{\rm KK} \sim \frac{1352\,\text{GeV}}{(\sin\theta_H)^{0.786}}, \quad m_{Z_R^{(1)}} \sim \frac{1038\,\text{GeV}}{(\sin\theta_H)^{0.784}}\ , \\
&m_{Z^{(1)}} \sim \frac{1044\,\text{GeV}}{(\sin\theta_H)^{0.808}}, \quad m_{\gamma^{(1)}} \sim \frac{1056\,\text{GeV}}{(\sin\theta_H)^{0.804}}\ , \\
&m_{t^{(1)}} \sim \frac{1033\,\text{GeV}}{(\sin\theta_H)^{0.862}}\ .
\end{aligned}
\tag{4.14}
$$

The fitting curves for Higgs self-couplings λ_3 and λ_4 are given by,

$$
\begin{aligned}
&\lambda_3/\text{GeV} = 26.7\cos\theta_H + 1.42(1+\cos 2\theta_H)\ , \\
&\lambda_4 = -0.0106 + 0.0304\cos 2\theta_H + 0.00159\cos 4\theta_H\ .
\end{aligned}
\tag{4.15}
$$

This relations mean that $m_{\rm KK}$, masses of $Z_R^{(1)}$, $Z^{(1)}$, $\gamma^{(1)}$ and $t^{(1)}$, couplings $g_{t_{L(R)}}^{Z^{(1)}}$, $g_{t_{L(R)}}^{Z^{(1)}}$, $g_{u_{L(R)}}^{Z^{(1)}}$ and $g_{d_{L(R)}}^{Z^{(1)}}$, λ_3 and λ_4 are independent on the detail of the dark fermion sector. This property is called the universality. The dark fermion parameters c_F and n_F have a important roll for determining the value of non-trivial minimum of the 1-loop Higgs effective potential whereas c_F and n_F are not important for some quantities which have universality. In sec.5.2 we analyze Z' search. We can use the parameter sets for $n_F = 5$ as a bench mark. The universality ensure that we need not to analyze other n_F. If quantities, for example $Z^{(1)}$ mass, are determined by experiments, we can know θ_H and other quantities by using the universality even though we do not know the detail of the dark fermion sector. On the

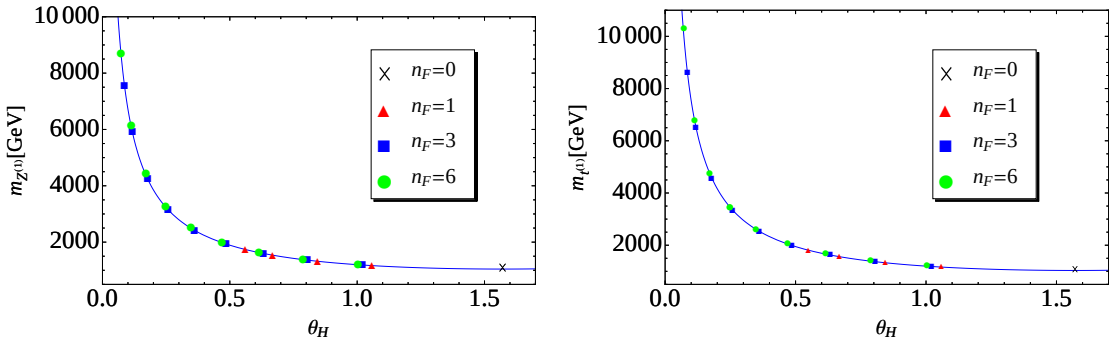

Figure 10: θ_H vs $m_{Z^{(1)}}$ and θ_H vs $m_{t^{(1)}}$ for $m_H = 126\,\mathrm{GeV}$ with n_F degenerate dark fermions in the left and right panels, respectively. Blue line in the left panel is fitting function $m_{Z^{(1)}} \sim 1044\,\mathrm{GeV}/(\sin\theta_H)^{0.808}$. Blue line in the right panel is fitting function $m_{t^{(1)}} \sim 1033\,\mathrm{GeV}/(\sin\theta_H)^{0.862}$. In the $n_F = 0$ case Wilson line phase is $\pi/2$. The left panel of this figure is originally shown in [13].

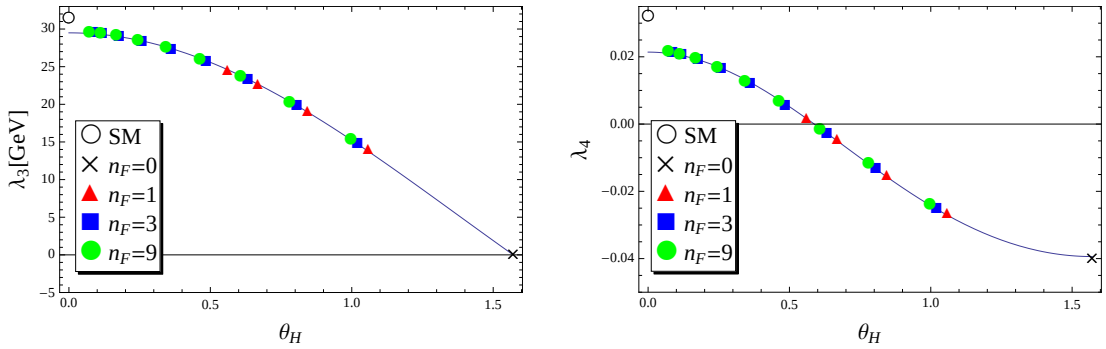

Figure 11: θ_H vs λ_3^H and λ_4^H for $m_H = 126\,\mathrm{GeV}$ with n_F degenerate dark fermions. In the SM $\lambda_3^{\mathrm{SM}} = 31.5\,\mathrm{GeV}$ and $\lambda_4^{\mathrm{SM}} = 0.0320$. The fitting curves are given by (4.15). These figures are originally shown in [13].

other hand, dark fermion mass has dependence of n_F, Fig.9. And we find that we cannot determine the detail of non-degenerate dark fermions from the θ_H m_{KK}, $m_{Z^{(1)}}$, Table 5 To determine the detail of dark fermions we should discuss searches for the dark fermions. In Sec.6 we discuss searches for the dark fermions with $Q_X = 1/2$ and predict the region θ_H in which dark fermions are discovered.

As we discussed the previous subsection, we regard the limit $\theta_H \to 0$ as the SM limit. Our Higgs self-coupling λ_3 and λ_4 for $\theta_H \to 0$ are small compared with those in the SM, Fig.11. In the SM the Higgs self-couplings are $\lambda_3^{\mathrm{SM}} = 31.5\,\mathrm{GeV}$ and $\lambda_4^{\mathrm{SM}} = 0.0320$. It is interesting to distinguish our Higgs self-couplings from those in the SM in the future experiments. At small θ_H the absolute value of the right-handed quark coupling with $Z^{(1)}$

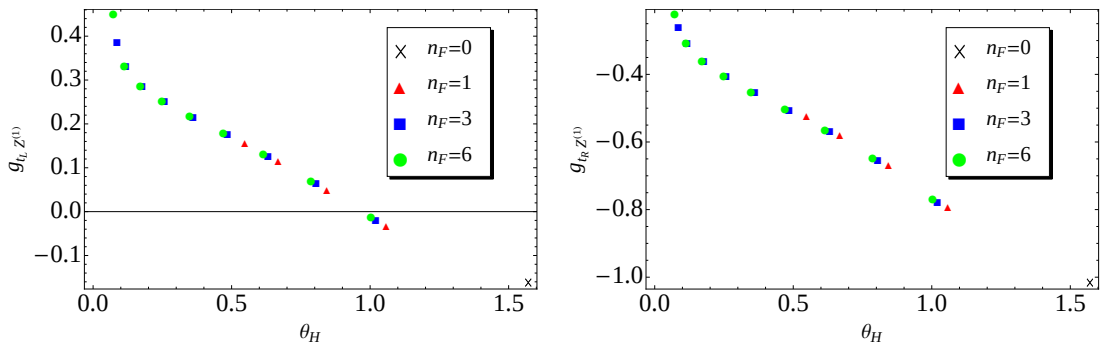

Figure 12: θ_H vs left-handed top quark coupling with $Z^{(1)}$ and θ_H vs right-handed top quark coupling with $Z^{(1)}$ for $m_H = 126\,\text{GeV}$ with n_F degenerate dark fermions in the left and right panels, respectively. In the $n_F = 0$ case Wilson line phase is $\pi/2$.

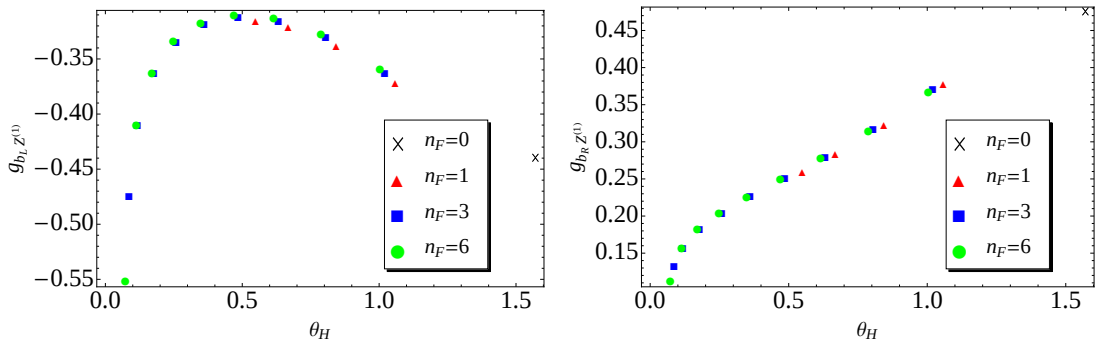

Figure 13: θ_H vs left-handed bottom coupling quark with $Z^{(1)}$ and θ_H vs right-handed bottom quark coupling with $Z^{(1)}$ for $m_H = 126\,\text{GeV}$ with n_F degenerate dark fermions in the left and right panels, respectively. In the $n_F = 0$ case Wilson line phase is $\pi/2$.

is smaller than that of $n_F = 0$ case. On the other hand, at small θ_H the absolute value of the left-handed quark coupling with $Z^{(1)}$ is larger than that of $n_F = 0$ case. In the case of $n_F = 0$ our Higgs cubic coupling is zero. Our Higgs quartic coupling λ_4 is negative for $\theta_H < 0.6$ and do not cause the instability. In the gauge-Higgs unification there is no instability problem in the Higgs couplings. For example Higgs effective potential $V_{\text{eff}}(\theta_H)$ for negative λ_4 and $\theta_H = \pi/2$ is the left panel in Fig.4.

We study the universality for various Higgs mass. In Fig.16 we plot the m_{KK} against θ_H. The KK mass scale m_{KK} increases as m_H. The fitting curve is parametrized by $m_{\text{KK}} = \alpha/|\sin\theta_H|^\beta$ with fixed m_H. The parameters α and β are tabulated in Table 7. We plot $m_{\text{KK}}(\theta_H)$ for $m_H = 110, 126, 140\,\text{GeV}$ in Fig. 16. The Higgs mass is measured to be $m_H = 125.3 \pm 0.4(\text{stat.}) \pm 0.5(\text{syst.})$ GeV and $m_H = 125.36 \pm 0.37(\text{stat}) \pm 0.18(\text{syst})$ GeV by the CMS collaborations and the ATLAS collaboration, respectively[2][3]. In our analysis

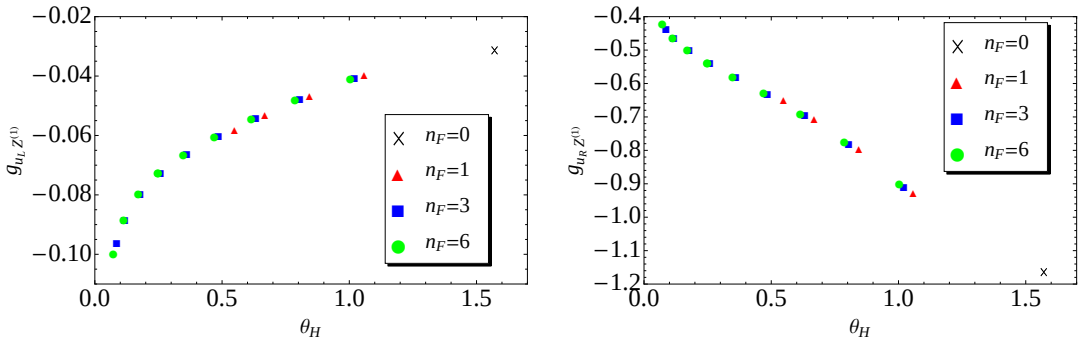

Figure 14: θ_H vs left-handed up quark coupling with $Z^{(1)}$ and θ_H vs right-handed up quark coupling with $Z^{(1)}$ for $m_H = 126\,\mathrm{GeV}$ with n_F degenerate dark fermions in the left and right panels, respectively. In the $n_F = 0$ case Wilson line phase is $\pi/2$.

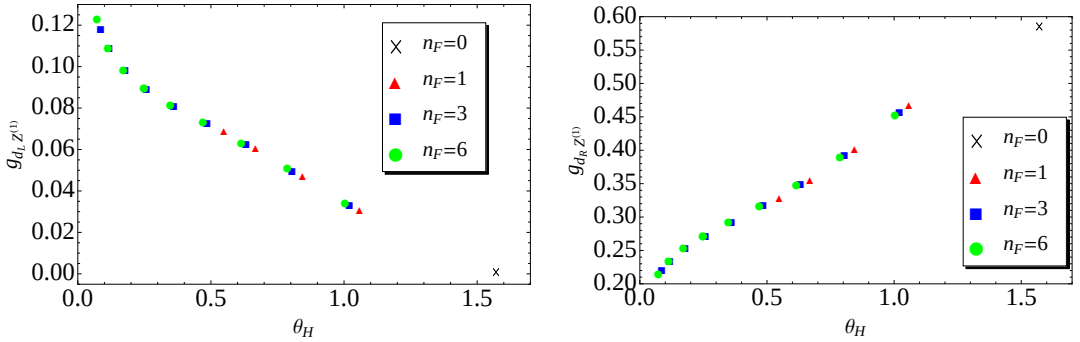

Figure 15: θ_H vs left-handed down quark coupling with $Z^{(1)}$ and θ_H vs right-handed down quark coupling with $Z^{(1)}$ for $m_H = 126\,\mathrm{GeV}$ with n_F degenerate dark fermions in the left and right panels, respectively. In the $n_F = 0$ case Wilson line phase is $\pi/2$.

we use $m_H = 126$ GeV. Fig.16 and Table 7 indicate that changing our result for Sec.5.1, 5.2 and 6 is sufficiently small to change the values between the measured Higgs mass and our Higgs mass.

We mention again that the universality leads to powerful predictions. Once the value of θ_H is determined from, say, $m_{Z^{(1)}}$, many other quantities are predicted. In Sec.5.2 we study the Z' search. Our $Z_R^{(1)}$, $Z^{(1)}$ and $\gamma^{(1)}$ become the Z' bosons. If these particles are discovered in the future experiments, our Higgs self-couplings are determined through determining θ_H by using the universality. Then if the Higgs self-couplings are determined by the future experiments, due to this property our model is distinguishable from other models beyond the SM.

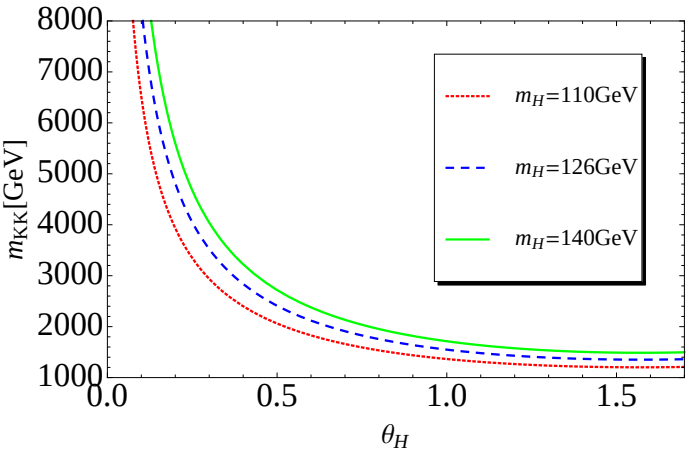

Figure 16: θ_H vs m_{KK} with various values of m_H. This figure is originally shown in [13].

Table 7: This table is shown in [13]. Universality relation $m_{\rm KK} = \alpha/|\sin\theta_H|^\beta$ with various value of m_H.

m_H(GeV)	α(TeV)	β
110	1.20	0.733
120	1.30	0.766
126	1.35	0.786
130	1.39	0.800
140	1.49	0.820

5 $SO(5) \times U(1)$ GHU in the LHC experiments

5.1 Higgs decay $H \to \gamma\gamma$

When Higgs boson was discovered, signal strength for $H \to \gamma\gamma$ is larger than that in the SM. In 2014 the signal strength of $H \to \gamma\gamma$ divided by the corresponding SM prediction is found the best-fit value $\mu = 1.17 \pm 0.27$ at the value of $m_H = 125.4$ GeV by ATLAS collaboration [20] and $\mu = 1.14^{+0.26}_{-0.23}$ at the value of $m_H = 124.7$ GeV by the CMS collaboration [21] in 8 TeV LHC experiments. $H \to \gamma\gamma$ has no tree level diagram. Dominant processes are loop diagrams. So it was expected that contributions of new physics may be hidden. In this subsection we summarize the result of [7].

5.1.1 Couplings for $H \to \gamma\gamma$

We evaluate Higgs couplings with W boson, top quark, dark fermions and their KK modes in Fig. 17. We calculate $HW^{(n)}W^{(n)\dagger}$ couplings $g_{HW^{(n)}W^{(n)}}$, Yukawa couplings $y_{t^{(n)}}$ and

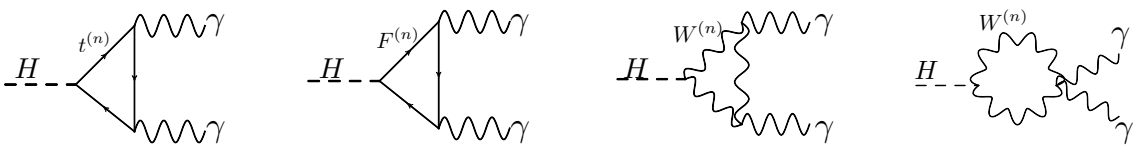

Figure 17: Diagram of $H \to \gamma\gamma$

$y_{F^{(n)}}$ and we define the ratios,

$$I_{W^{(n)}} = \frac{g_{HW^{(n)}W^{(n)}}}{g_w m_{W^{(n)}} \cos\theta_H} = -\sqrt{kL(z_L^2-1)}\,\frac{\sin\theta_H}{r_{W^{(n)}}}\,\frac{C(1;\lambda_{W^{(n)}})}{S(1;\lambda_{W^{(n)}})}, \tag{5.1}$$

$$I_{t^{(n)}} = \frac{y_{t^{(n)}}}{y_t^{\rm SM}\cos\theta_H} = -\frac{g_w}{2y_t^{\rm SM}}\sqrt{kL(z_L^2-1)}\,\frac{\sin\theta_H}{r_{t^{(n)}}}\,\frac{C_L(1;\lambda_{t^{(n)}},c_t)}{S_L(1;\lambda_{t^{(n)}},c_t)}, \tag{5.2}$$

$$I_{F^{(n)}} = \frac{y_{F^{(n)}}}{y_t^{\rm SM}\sin\frac{1}{2}\theta_H} = -\frac{g_w}{4y_t^{\rm SM}}\sqrt{kL(z_L^2-1)}\,\frac{\cos\frac{1}{2}\theta_H}{r_{F^{(n)}}}\,\frac{C_R(1;\lambda_{F^{(n)}},c_F)}{S_R(1;\lambda_{F^{(n)}},c_F)}. \tag{5.3}$$

where $g_{HWW}^{\rm SM}$ and $y_t^{\rm SM}$ are HWW and the top Yukawa couplings in the SM, respectively. These ratios are plotted in Fig.18 for $n_F = 3$ and $z_L = 10^8$ ($\theta_H = 0.360$). The signs of $I_{W^{(n)}}$, $I_{t^{(n)}}$ and $I_{F^{(n)}}$ alternate as n increase. The magnitudes of $I_{W^{(n)}}$, $I_{t^{(n)}}$ and $I_{F^{(n)}}$ are almost constant.

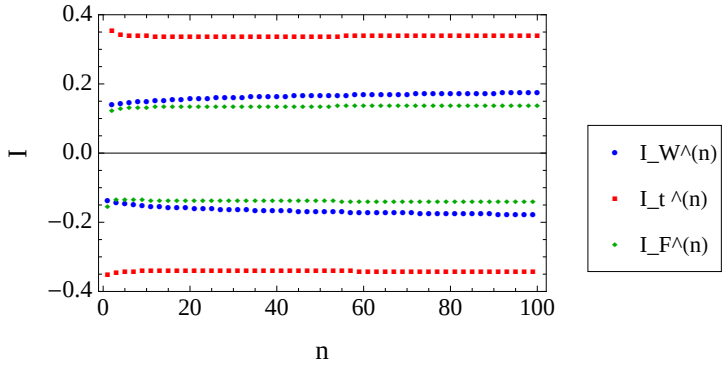

Figure 18: The ratios $I_{W^{(n)}} = g_{HW^{(n)}W^{(n)}}/g_w m_{W^{(n)}}\cos\theta_H$ in (5.1), $I_{t^{(n)}} = y_{t^{(n)}}/y_t^{\rm SM}\cos\theta_H$ in (5.2) and $I_{F^{(n)}} = y_{F^{(n)}}/y_t^{\rm SM}\sin\frac{1}{2}\theta_H$ in (5.3) are plotted for $n_F = 3$ and $\theta_H = 0.360$ ($z_L = 10^8$) in the range $1 \le n \le 100$. ($\square$: the top quark tower, $\Diamond$: the W tower, $\bigcirc$: the Ψ_F tower) $I_{W^{(0)}} = 1.004$ and $I_{t^{(0)}} = 1.012$. The sign of $g_{HW^{(n)}W^{(n)}}$, $y_{t^{(n)}}$ and $y_{F^{(n)}}$ alternates as n increases. $I_{W^{(1)}}, I_{t^{(1)}}, I_{F^{(1)}} < 0$. This figure is originally shown in [7].

Table 8: Functions $\mathcal{F}_W$, $\mathcal{F}_{\rm top}$ and $\mathcal{F}_F$ in the $n_F = 3$ and $z_L = 10^5, 10^8$ case. This suggests most of the contributions come from the lowest modes of the top quark and W boson. Contributions of the W boson and the top quark are denoted by $\mathcal{F}_{W\,\rm only}$ and $\mathcal{F}_{\rm top\ only}$, respectively. We obtain $\mathcal{F}_W + \frac{4}{3}\mathcal{F}_{\rm top} + \frac{3}{2}\mathcal{F}_F = 6.508$ and 6.199 for $\theta_H = 0.117$ and 0.360.

z_L	θ_H	$\mathcal{F}_{W\,\rm only}$	$\mathcal{F}_{\rm top\ only}$	$\mathcal{F}_W/\mathcal{F}_{W\,\rm only}$	$\mathcal{F}_{\rm top}/\mathcal{F}_{\rm top\ only}$	$\mathcal{F}_F/\mathcal{F}_{\rm top\ only}$
10^8	0.360	7.873	-1.305	0.998	0.990	-0.033
10^5	0.117	8.330	-1.372	0.9996	0.998	-0.0034

5.1.2 Decay rate for $H \to \gamma\gamma, gg$

The decay rate is given by [22]-[24],

$$\Gamma(H \to \gamma\gamma) = \frac{\alpha^2 g_w^2}{1024\pi^3}\frac{m_H^3}{m_W^2}\left|\mathcal{F}_W + \frac{4}{3}\mathcal{F}_{\rm top} + \left(2(Q_X^{(F)})^2 + \frac{1}{2}\right) n_F \mathcal{F}_F\right|^2 ,$$

$$\mathcal{F}_W = \sum_{n=0}^{\infty} \frac{g_{HW^{(n)}W^{(n)}}}{g_w\, m_W}\frac{m_W^2}{m_{W^{(n)}}^2} F_1(\tau_{W^{(n)}}) ,$$

$$\mathcal{F}_{\rm top} = \sum_{n=0}^{\infty} \frac{y_{t^{(n)}}}{y_t^{\rm SM}}\frac{m_t}{m_{t^{(n)}}} F_{1/2}(\tau_{t^{(n)}}) ,$$

$$\mathcal{F}_F = \sum_{n=1}^{\infty} \frac{y_{F^{(n)}}}{y_t^{\rm SM}}\frac{m_t}{m_{F^{(n)}}} F_{1/2}(\tau_{F^{(n)}}) , \tag{5.4}$$

where $W^{(0)} = W$, $t^{(0)} = t$, $\tau_a = 4m_a^2/m_H^2$ and the functions $F_1(\tau)$ and $F_{1/2}(\tau)$ are defined in Ref. [24]. $Q_X^{(F)}$ is the $U(1)_X$ charge of Ψ_F. For large mass limit, $\tau \to \infty$, $F_1(\tau)$ and $F_{1/2}(\tau)$ behave $F_1(\tau) \to 7$ and $F_{1/2}(\tau) \to -\frac{4}{3}$. The dark fermion multiplet Ψ_F contains particles with electric charges $(Q_X^{(F)} \pm \frac{1}{2})e$.

The infinite sums in $\mathcal{F}$s converge. The couplings alternate as KK mode n increase, Fig.18. All KK masses are proportional to $nm_{\rm KK}$. For large mass limit, $\tau \to \infty$, $F_1(\tau)$ and $F_{1/2}(\tau)$ behave constant. Therefore the infinite sums converge as $\mathcal{F} \sim \sum(-1)^n n^{-1}$ or $\sum(-1)^n n^{-1}(\ln n)^q$ $(q = 1, 2, \cdots)$.

We calculate amplitudes $\mathcal{F}$s numerically. We tabulate the result of $\mathcal{F}$s for $n_F = 3$, $z_L = 10^5$ and 10^8 ($\theta_H = 0.117$ and 0.360) and $Q_X = 0$ in Table 8. The ratio of all contributions divided by those of the only W boson and the top quark is 1.001 and 1.011 for $\theta_H = 0.117$ and 0.360. Therefore contributions of KK modes and the dark fermions are small, i.e. contributions of KK modes are 0.1% (1.1%) for θ_H =0.117 (0.360).

In the GHU, Higgs couplings with WW, ZZ, $c\bar{c}$, $b\bar{b}$ and $\tau\bar{\tau}$ are $\cos\theta_H$ compared with those in the SM (i.e. $g_{\rm GHU} \sim g_{\rm SM}\cos\theta_H$). So all decay rates are suppressed by $\cos^2\theta_H$.

Branching fraction for the Higgs boson is defined by the ratio $\Gamma(Higgs \to X)/\Gamma(Higgs \to all)$. In this form the factor $\cos^2\theta_H$ is cancelled. The signal strength is determined by the product of the Higgs production rate and the branching fraction. Because the Higgs production rate is proportional to $\cos^2\theta_H$, the GHU predicts that the signal strength relative to the SM is $\sim \cos^2\theta_H$. For $\theta_H = 0.1\,(0.3)$, the signal strength relative to the SM is about 0.99 (0.91). This result is consistent with the result of the LHC experiments.

5.2 Z' search

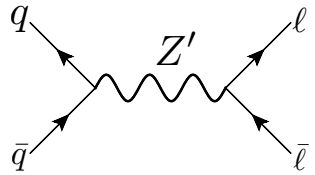

Figure 19: Diagram Z'. Our Z's are $Z^{(1)}$, $\gamma^{(1)}$ and $Z_R^{(1)}$.

We predict the new particles which come from the extra dimension at 14 TeV LHC experiments[13]. First exited modes of Z boson $Z^{(1)}$, photon $\gamma^{(1)}$, the lowest mode of Z_R and $Z_R^{(1)}$ have TeV scale mass in the $SO(5) \times U(1)$ GHU. The masses $Z_R^{(1)}$, $Z^{(1)}$ and $\gamma^{(1)}$ and couplings of quarks with $Z^{(1)}$ have universality in Fig.10 and 12–15. According to Fig. 10 these masses are 3 - 6 TeV for $\theta_H = 0.1$ - 0.2. These massive neutral gauge bosons appear as the Z' boson. There are no signal of Z' boson in the experiments [28]-[30]. Tree level diagram is Fig.19. In this section we summarize the result of [13].

5.2.1 Couplings and decay widths

Firstly we discuss our Z' couplings with quarks and leptons. The gauge couplings are shown in [13] . We tabulate the numerical results of $Z_R^{(1)}$, $Z^{(1)}$, $\gamma^{(1)}$ and $Z^{(2)}$ couplings in Table 9 and Table 10. We analyze only $n_F = 5$ case because these couplings have universality (See subection 4.2.). Because masses of $Z^{(1)}$ and $\gamma^{(1)}$ are almost the same, the resonances of $Z^{(1)}$ and $\gamma^{(1)}$ are located on almost the same invariant mass. Mass of the second KK Z boson is also TeV scale. However $Z^{(2)}$ coupling is smaller than that in the SM Z boson. As a result, the decay width of $Z^{(2)}$ is narrow. The wave functions of right-handed fermions and KK gauge bosons, $Z_R^{(1)}$, $Z^{(1)}$ and $\gamma^{(1)}$, localize on TeV brane. On

the other hand, the wave functions of left-handed fermions localize on the Planck brane. When we determine the couplings, we integrate over the fifth-dimensional part of wave functions. KK gauge boson couplings with right-handed fermions are larger than couplings with the left-handed fermions because wave functions of KK gauge bosons overlap that of right-handed fermions.

The decay width is tabulated in Table 9 and Table 10. The formula of the decay width is shown in the [13]. One finds that decay widths of $Z_R^{(1)}$, $Z^{(1)}$ and $\gamma^{(1)}$ are wider than decay width of the SM Z boson because the $Z_R^{(1)}$, $Z^{(1)}$ and $\gamma^{(1)}$ couplings with right-handed fermions are larger than that of the SM Z boson. The decay widths of $Z_R^{(1)}$, $Z^{(1)}$ and $\gamma^{(1)}$ are 300 - 900 GeV. This width is the characteristic signal of the $SO(5) \times U(1)$ GHU.

Table 9: Masses, total decay widths and couplings of the Z' bosons to SM particles in the first generation for $\theta_H = 0.114$. Couplings to μ are approximately the same as those to e. This table is originally shown in [13].

Z'	m(TeV)	Γ(GeV)	$g_{uL}^{Z'}$	$g_{dL}^{Z'}$	$g_{eL}^{Z'}$	$g_{uR}^{Z'}$	$g_{dR}^{Z'}$	$g_{eR}^{Z'}$
Z	0.0912	2.44	0.257	-0.314	-0.200	-0.115	0.0573	0.172
$Z_R^{(1)}$	5.73	482	0	0	0	0.641	-0.321	-0.978
$Z^{(1)}$	6.07	342	-0.0887	0.108	0.0690	-0.466	0.233	0.711
$\gamma^{(1)}$	6.08	886	-0.0724	0.0362	0.109	0.846	-0.423	-1.29
$Z^{(2)}$	9.14	1.75	-0.00727	0.00889	0.00565	-0.00548	0.00274	0.00856

Table 10: Masses, total decay widths and couplings of the Z' bosons to SM particles in the first generation for $\theta_H = 0.073$. This table is originally shown in [13].

Z'	m(TeV)	Γ(GeV)	$g_{uL}^{Z'}$	$g_{dL}^{Z'}$	$g_{eL}^{Z'}$	$g_{uR}^{Z'}$	$g_{dR}^{Z'}$	$g_{eR}^{Z'}$
$Z_R^{(1)}$	8.00	553	0	0	0	0.588	-0.294	-0.896
$Z^{(1)}$	8.61	494	-0.100	0.123	0.0780	-0.426	0.213	0.650
$\gamma^{(1)}$	8.61	1.04×10^3	-0.0817	0.0408	0.123	0.775	-0.388	-1.18
$Z^{(2)}$	12.8	1.33	-0.0540	0.00660	0.00420	-0.00433	0.00216	0.00675

5.2.2 Production at LHC

In our study, we calculate the dilepton production cross sections through the Z' boson, the Z boson and photon exchange, Fig.19. Formula of the dilepton production cross sections

is shown in [13]. We calculate the case of the final state $\mu^+\mu^-$. (The case of the final state e^+e^- is the similar result of $\mu^+\mu^-$ case.) We calculate the differential cross section for $pp \to \mu^+\mu^-$ for $n_F = 5$ at 8 TeV LHC experiments, Fig.20. The black doted line represents the SM background. The case of $\theta_H = 0.114$ (the red solid curve) is consistent with the SM. For the case of $\theta_H = 0.251$ (the blue dashed curve), the masses and the decay widths of $Z_R^{(1)}$,$Z^{(1)}$ and $\gamma^{(1)}$ are (341, 3.11), (221, 3.24) and (629 GeV, 3.24 TeV), respectively. The masses of Z' bosons in our model are heavier than the plot range of Fig. 20. The case of $\theta_H = 0.251$ (blue dashed curve) deviates from the SM background because of the wide tail of resonances for our Z'. The case of $\theta_H = 0.251$ (blue dashed curve) at $M_{\mu\mu} = 2$ TeV is 87 times larger than the SM background. The region $\theta_H < 0.13$ is consistent with the 8 TeV LHC experiments. In this region $Z_R^{(1)}$ mass is larger than 5.1 TeV.

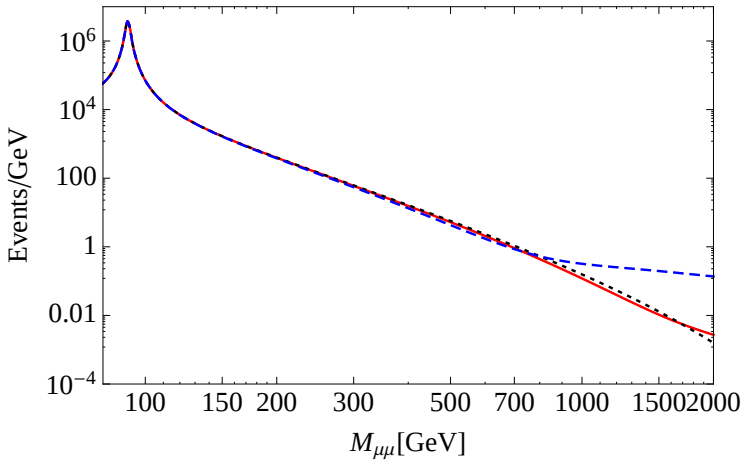

Figure 20: The differential cross section multiplied by an integrated luminosity of 20.6 fb^{-1} for $pp \to \mu^+\mu^- X$ at the 8 TeV LHC for $\theta_H = 0.114$ (red solid curve) and for $\theta_H = 0.251$ (blue dashed curve). The black dashed line represents the SM background. This figure is originally shown in [13].

We predict the signal of $pp \to \mu^+\mu^-$ at 14 TeV LHC experiments. In Fig.21 the differential cross section $d\sigma/dM_{\mu\mu}$ for $\theta_H = 0.114$ and 0.073 ranges $3\,\text{TeV} < M_{\mu\mu} < 9\,\text{TeV}$. Masses and decay widths of our Z' bosons are tabulated in Table 9 and Table 10. There are two peaks and the large tail of resonances for $Z_R^{(1)}$,$Z^{(1)}$ and $\gamma^{(1)}$. This signal deviates from the SM. Therefore this signal can be detected at the upgraded LHC. At $M_{\mu\mu} = 3$ TeV (4 TeV) the case of $\theta_H = 0.114$ (the red solid line) are 13 (86) times as large as the SM. For $\theta_H = 0.114$, an excess due to the broad widths of the Z' resonances should be observed

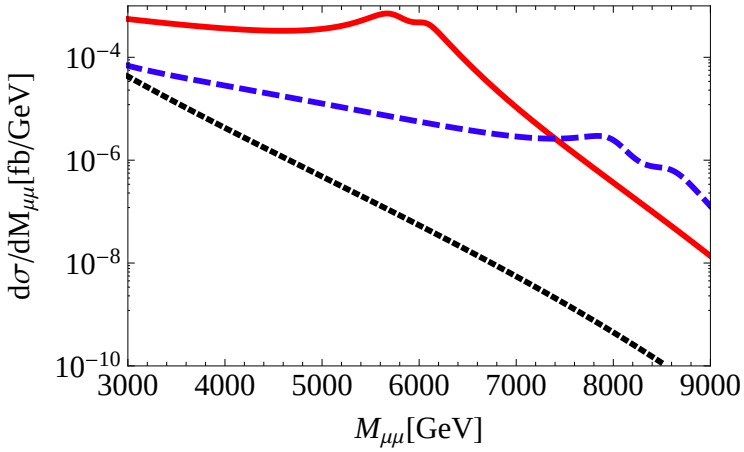

Figure 21: The differential cross section for $pp \to \mu^+\mu^- X$ at the 14 TeV LHC for $\theta_H = 0.114$ (red solid curve) and for $\theta_H = 0.073$ (blue dashed curve) . The nearly straight line represents the SM background. This figure is originally shown in [13].

above 3 TeV in the dilepton invariant mass. The discovery of the Z' bosons in the 3-9 TeV range would give strong support for the GHU. Furthermore this is the signals of the existence of extra dimensions. However we cannot know the detail of the dark fermions. In the next section we study the dark fermions as a candidate of dark matters. The number of dark fermions n_F and θ_H can be constrained by the relic density of dark matter and direct searches.

6 Dark fermion as a dark matter candidate

The dark matter is required by observations of the cosmology. We summarize the result of our paper [14]. In the $SO(5) \times U(1)$ GHU the lightest neutral component of dark fermions can become one of the candidate of the dark matter. When we take $U(1)_X$ charge $Q_X = 1/2$, we have neutral and charged components of dark fermions. The charged dark fermions are heavier than the neutral dark fermions due to loop contributions. The charged dark fermions decay sufficiently fast, these fermions do not exist in the present universe. In this section we consider constraints from relic density [31] and direct detections [32][33].

We analyze the dark matter decay until the freeze-out temperature. In the $SO(5)\times U(1)$ GHU we consider both neutral and charged dark fermions. The charged dark fermion contributes as coannihilation. The couplings of the dark fermions are very weak compared with the SM particle for small θ because the dark fermion couplings are proportional to $\sin\theta_H$. In this situation it may be difficult that the dark fermions decay. However decays of

the dark fermions are enhanced by the Breit-Wigner resonance. The strong enhancement occurs at $m_{Z_R^{(1)}} \sim 2m_F$. On the other hand, the number of the dark fermions is the suppression factor for cross section because one of the dark fermions can only decay with the pair of the dark fermion. Therefore this suppression factor is $1/2n_F$ which $1/2$ comes from the contribution of the antiparticle because the dark fermion is Dirac dark matter.

The dark matter is also searched directly by using collisions with nuclei. In recent years the constraints for cross section of dark matter with nuclei become strong by experiments. In the $SO(5) \times U(1)$ GHU main processes of the dark fermions with nucleus are Z, $Z_R^{(1)}$ and Higgs exchange processes. We find that we have a region which is consistent with the experiments of the relic density and direct search.

6.1 The neutral and charged dark fermions

Firstly we introduce the dark fermions with $Q_X = 1/2$ in Sec.3.2. This dark fermion has the charged ($Q_{\rm EM} = 1$) and neutral ($Q_{\rm EM} = 0$) components. According to our analysis of Z' search, θ_H ranges 0.1 - 0.2. In this region the lowest mode of Ψ_{F_i} has the mass range 1.5 - 4 TeV. For small θ_H the dark fermions with the boundary condition $\eta_{F_i} = +1$ couple to $SU(2)_L$ bosons very weakly. On the other hand, for small θ_H the dark fermions with the boundary condition $\eta_{F_i} = -1$ couple to $SU(2)_R$ bosons very weakly. The dark fermion number is conserved so that the lightest mode of the dark fermions becomes stable. The charged and neutral components of the dark fermions have the same mass at tree-level. The charged components of the dark fermion are heavier than the neutral components of the dark fermion because of the radiative correction depicted in Fig.22. The mass difference of dark fermions must be the order of 10GeV or larger. More detail of this mass difference between the charged and neutral components of the dark fermion is shown in Ref.[14]. Hereafter we assume that charged components of dark fermions decay to neutral components of the dark fermions sufficiently quickly. In the present universe only the neutral components of dark fermions are left. We consider the both contributions of the charged and neutral components in the relic abundance of the dark matter. On the other hand, we consider the contribution from only the neutral components of the dark fermion in the direct detection of the dark matter.

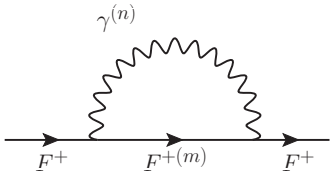

Figure 22: Diagrams contributing to the fermion mass difference $\Delta m_F = \delta m_{F^+} - \delta m_{F^0}$. This figure is originally shown in [14].

6.2 Relic density

The best value [68% confidence level (CL) limits] of the relic density of the cold dark matter observed by Planck [31]:

$$\Omega_{\rm CDM}h^2 \;=\; 0.11805 \quad [0.1186 \pm 0.0031], \tag{6.1}$$

where Hubble's expansion-rate $H_0 \equiv 100h\,{\rm km\,s^{-1}Mpc^{-1}}$, $100h = 67.11$ $[67.4 \pm 1.4]$.

We analyze the relic abundance of the dark matter in the early universe [34]-[36]. To know the time evolution of $n_{(F)}$ which denotes the number density of F, we consider the Boltzmann equation for F_i^0.

6.2.1 Pair annihilations and relic density of dark fermions

We consider the case where θ_H is small ($z_L \lesssim 10^6$, $\theta_H < 0.2$) because of the result for Z' search (Sec.5.2). In such a case, $m_{\rm KK}$ is about 5.5 TeV $\sim$ 10.5 TeV and dark fermion becomes heavy. Because of the dark fermion coupling is proportional to $\sin\theta_H$, some of annihilation amplitudes are processes are suppressed by $\sin^2\theta_H$. Relevant processes for dark fermion annihilation are the following s-channel processes

$$\begin{array}{ccccc} F^0\bar{F}^0 & \to & Z_R^{(1)} & \to & q\bar{q},\, l\bar{l},\, \nu\bar{\nu}, \\ F^+F^- & \to & \gamma,\, \gamma^{(1)} & \to & q\bar{q},\, l\bar{l}, \\ F^+F^- & \to & Z_R^{(1)} & \to & q\bar{q},\, l\bar{l},\, \nu\bar{\nu}, \end{array} \tag{6.2}$$

and all other annihilation and co-annihilation processes are negligible. This detail is shown in Ref.[14]

Now we calculate the relic density of the degenerate dark fermions numerically. Parameter sets are obtained in Sec.4, Table 2 and Table 11. In Fig.23 we plot the relic density of the dark fermion for $n_F = 3, 4, 5$ and 6. In the case of the $n_F = 3$ the relic density is smaller than the current observed limit. Especially in the case of $n_F = 3$ and $z_L \sim 3 \times 10^4$ the relic density become small because of the Breit–Wigner resonance. On the other hand,

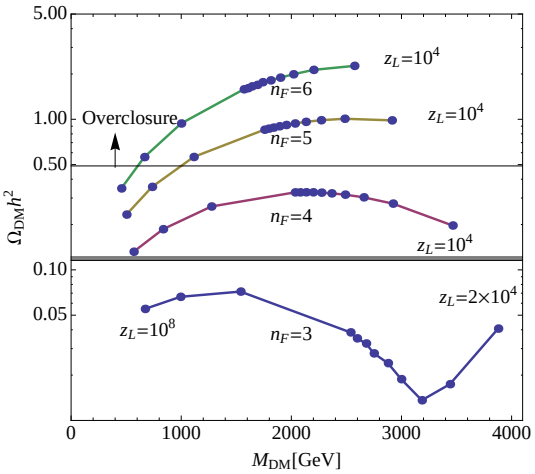

Figure 23: Relic density of neutral dark fermions in the case of n_f degenerate dark fermion multiplets ($n_F = 3, 4, 5, 6$). Data points are, from right to left, $z_L = 10^4$ (2×10^4) to 10^5 with a step of 10^4, 10^6, 10^7 and 10^8 for $n_F = 4, 5, 6$ ($n_F = 3$). The current observed limit of $\Omega_{\rm DM}h^2$ and the lower bound of the over-closure of the universe are indicated as horizontal lines. This figure is originally shown in [14].

in the case of the $n_F = 4, 5$ and 6, the relic density is larger than the current observed limit. We find that for the degenerate dark fermion case we do not explain the current DM density.

6.2.2 The case of the non-degenerate dark fermions

We consider the two types of dark fermions. Some of the dark fermions are heavier, the others are lighter. The mass difference of these dark fermions is $O(100)$ GeV (See Sec.4.). Only the lightest $F_i^{0(1)}$'s become the dark matter. Heavier one is needed to decay sufficiently fast. The lowest modes of heavy and light dark fermions denote (F_h^+, F_h^0) and (F_l^+, F_l^0), respectively. The lighter dark fermions obeys the boundary condition $\eta_{F_l} = +1$, whereas heavier dark fermions obeys the boundary condition $\eta_{F_h} = -1$. For small θ_H the lowest mode $(F_h^{+(1)}, F_h^{0(1)})$ strongly couples to an $SU(2)_L$ doublet compared with an $SU(2)_R$ doublet. On the other hand, for small θ_H, $(F_l^{+(1)}, F_l^{0(1)})$ strongly couples to an $SU(2)_R$ doublet compared with an $SU(2)_L$ doublet. Heavier neutral dark fermions F_h^0 can decay as shown in Fig. 24. Hereafter we assume that heavy dark fermions decay to light dark fermions sufficiently quickly. More detail of the mass difference for the non-degenerate dark fermion is shown in Ref.[14].

The heavy dark fermion couplings with W and Z bosons are not small. Therefore the dominant annihilation processes of F_h are s-channel processes of $F\bar{F}$ annihilation to the

Table 11: θ_H, $c_{\rm top}$, c_F and m_F for z_L and $n_F = 4, 5$ and 6, in the case of where dark fermions are degenerate. This table is originally shown in [14].

n_F	z_L	θ_H	$c_{\rm top}$	c_F	m_F [TeV]
4	10^8	0.355	0.357	0.423	0.567
	10^6	0.174	0.292	0.374	1.27
	10^5	0.115	0.227	0.332	2.03
	3×10^4	0.0917	0.168	0.299	2.66
	10^4	0.0737	0.0366	0.256	3.46
6	10^8	0.348	0.356	0.461	0.455
	10^6	0.171	0.292	0.434	1.00
	10^5	0.113	0.227	0.414	1.57
	10^4	0.0724	0.0365	0.379	2.57

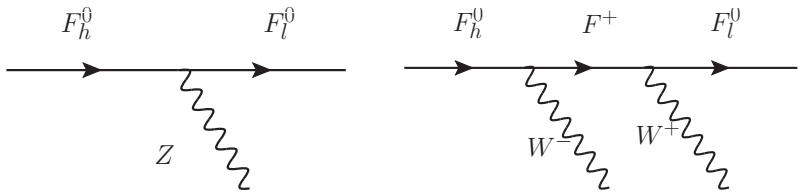

Figure 24: F_h^0 decay to F_l^0 by emitting one Z boson or two W bosons. This figure is originally shown in [14].

Table 12: Parameters in the non-degenerate case of dark fermions, $(n_{\rm light}, n_{\rm heavy})$. Bulk mass parameter c_{F_l} and the masses m_{F_h} and m_{F_l} of F_h and F_l are tabulated for various $\Delta c_F \equiv c_{F_l} - c_{F_h}$ (see text) and z_L. Even small Δc_F gives rise to large mass difference. This table is originally shown in [14].

Δc_F		0.04			0.06		
$(n_{\rm light}, n_{\rm heavy})$	z_L	c_{F_l}	m_{F_h} [TeV]	m_{F_l} [TeV]	c_{F_l}	m_{F_h} [TeV]	m_{F_l} [TeV]
(1,3)	10^6	0.404	1.32	1.13	0.418	1.34	1.06
	10^5	0.362	2.09	1.86	0.377	2.12	1.77
	3×10^4	0.329	2.72	2.46	0.344	2.76	2.36
	10^4	0.286	3.54	3.24	0.240	3.58	3.14
(2,2)	10^5	0.352	2.15	1.92	0.361	2.21	1.86
	10^4	0.276	3.61	3.32	0.285	3.69	3.25
(3, 1)	10^5	0.342	2.21	1.98	0.346	2.30	1.95
	10^4	0.266	3.68	3.39	0.270	3.80	3.36

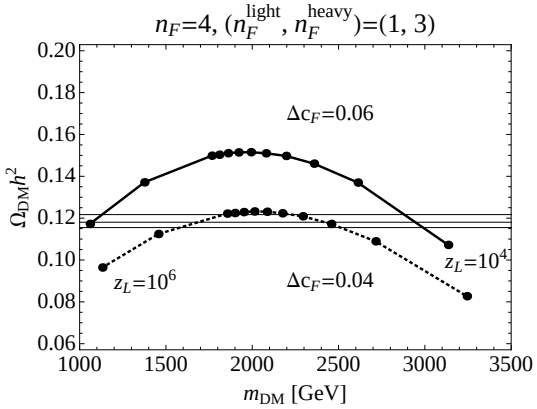

Figure 25: Relic density of the dark fermion versus $m_{\rm DM} = m_{F_l}$ for $n_F = 4$ ($n_{\rm light} = 1, n_{\rm heavy} = 3$). Thick-solid and thick-dotted lines are $\Delta c_F \equiv c_{F_l} - c_{F_h} = 0.06$ and 0.04, respectively. Data points are, from right to left, $z_L = 10^4$ to 10^5 with an interval 10^4, 3×10^5 and 10^6. Horizontal lines around $\Omega_{\rm DM}h^2 \sim 0.12$ show the observed 68% confidence level (CL) limit of the relic density of the cold dark matter. This figure is originally shown in [14].

SM fermions through $Z^{(1)}$ and $\gamma^{(1)}$ and co-annihilation through $W^{(1)}$. Through the similar procedure of the degenerate dark fermion case we can analyze the Boltzmann equation and the annihilation cross section of the dark fermions. We denote mass difference

$$\eta = \frac{m_{F_h} - m_{F_l}}{m_{F_l}}. \tag{6.3}$$

In our analysis, the annihilation cross section of the non-degenerate dark fermions is suppressed by a factor $n_F/n_F^{\rm light}$ compared with that of the degenerate dark fermions. As the number of the heavy dark fermions increases, The annihilation cross section becomes small and the relic abundance enhances.

We find that the current observed relic abundance in the parameter sets of the $(n_F^{\rm light}, n_F^{\rm heavy}) = (1, 3)$ is reconstructed, Fig.25. The other parameter sets cannot do. In the case of $\Delta c_F = 0.04$ and $\Delta c_F = 0.06$ corresponding mass differences are about 300 GeV and about 400 GeV, respectively, Table 12. Note that the small mass regions (less than 1000 GeV) is inconsistent with the result of the Z' search.

We plot the relic abundance in $(\Delta c_F, z_L)$ plane to interpolate and extrapolate with respect Δc_F and z_L, Fig.26. Inner and outer colored regions are allowed with the 68% CL limit and twice of the 68% CL limit $\Omega_{\rm DM}h^2 \subset [0.1186 \pm 2 \times 0.0031]$, respectively. We obtain the current observed relic abundance in the parameter region $10^4 \lesssim z_L \lesssim 10^6$ and $0.04 \lesssim \Delta c_F \lesssim 0.07$. The small z_L regions (less than 10^6) is inconsistent with the result of the Z' search. The corresponding regions of the Wilson line phase and the dark fermion mass are $0.07 \lesssim \theta_H \lesssim 0.17$ and $3100 \lesssim m_F \lesssim 1000$ GeV, respectively.

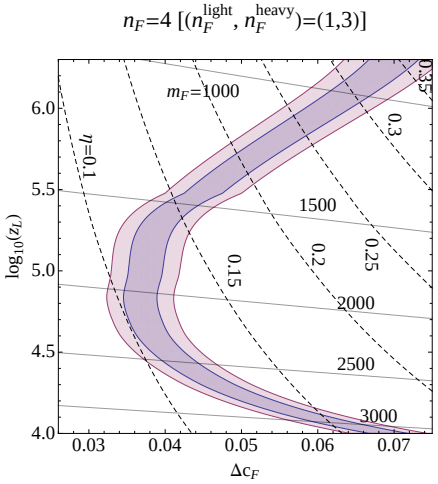

Figure 26: Parameter region $(\Delta c_F, z_L)$ allowed by the limits of relic density. Inner and outer colored regions are allowed with the 68% CL limit and twice of the 68% CL limit $\Omega_{\rm DM}h^2 \subset [0.1186 \pm 2 \times 0.0031]$, respectively. Mass of the dark fermion m_{F_l} and a mass ratio $\eta \equiv (m_{F_h} - m_{F_l})/m_{F_l}$ are also indicated as solid and dashed lines, respectively. This figure is originally shown in [14]

.

6.3 Direct detection

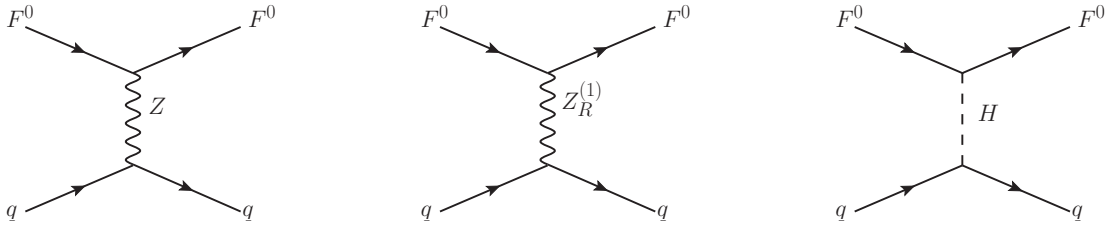

Figure 27: Dominant and subdominant processes of the F^0-nucleus scattering. This figure is originally shown in [14].

Let us analyze the elastic scattering between the dark fermion (F^0) and a nucleus [37]-[39]. We examine the constraint coming from direct detection experiments[32][33]. We treat only the neutral dark fermion F^0 because the charged dark fermion does not exist in the present. The dominant process is the Z boson exchange, Fig.27. The subdominant processes are $Z_R^{(1)}$ and Higgs exchange. Because the F^0 coupling to Z boson is small, and the $Z_R^{(1)}$ mass is heavy, contributions of Z and $Z_R^{(1)}$ boson are small so that the dark fermions are not observed by the current direct search.

Heavy target nuclei are used by the experiments [32][33]. These experiments are the spin-independent scattering experiments. More detail of the F^0-nucleon spin-independent

Table 13: F^0 mass m_F and the spin-independent cross section σ_N of the F^0-nucleon scattering for $n_F = 4, 5, 6$ degenerate dark fermions. This figure is originally shown in [14].

$n_F = 4$

z_L	θ_H	m_F (TeV)	σ_N (cm^2)
10^5	0.115	2.03	5.33×10^{-44}
5×10^4	0.101	2.36	3.78×10^{-44}
3×10^4	0.092	2.66	2.99×10^{-44}
2×10^4	0.085	2.92	2.53×10^{-44}
10^4	0.074	3.46	2.03×10^{-44}

$n_F = 5$

z_L	θ_H	m_F (TeV)	σ_N (cm^2)
10^5	0.114	1.75	3.67×10^{-44}
10^4	0.073	2.91	1.01×10^{-44}

$n_F = 6$

z_L	θ_H	m_F (TeV)	σ_N (cm^2)
10^5	0.113	1.57	2.96×10^{-44}
10^4	0.072	2.56	0.72×10^{-44}

cross sections σ_N is in ref. [14]. Our numerical result of the F^0-nucleon spin-independent cross sections σ_N are shown in Table 13 and Fig. 28. In Fig. 28 the black solid line is the strongest bound for current direct dark matter direct search and the 90% confidence limits set by the 85.3 live-days result of the LUX experiment[33]. The black doted line is the bound of the expectation values by the 300 live-days result of the LUX experiment. Red circles and blue squares represent the cases of non-degenerate dark fermions $(n_{\text{light}}, n_{\text{heavy}}) = (1, 3)$ with $\Delta c_F = 0.04$ and 0.06, respectively. The purple and light purple bands represent the regions allowed by the limit of the relic abundance of dark matter at the 68 % CL and by twice of that, respectively. When we choose the suitable mass difference Δc_F, our result are consistent with the dark matter direct search. This band indicates the allowed region for both relic density and direct detection of dark fermions exists. Thus the allowed band region is from $z_L = 10^4$ to 4×10^4, from $m_F = 3.1$ TeV to 2.3 TeV and from $\theta_H = 0.074$ to 0.097. In this band the mass of Z' bosons ranges from 8 TeV to 6.5 TeV. Therefore we find that this allowed region is consistent with the relic density, direct search and the results of Higgs decay and Z' search.

Table 14: m_{F_l}, $m_{Z_R^{(1)}}$, the spin-independent cross section σ_N of the F_l^0-nucleon scattering for $n_F = 4$ and $(n_{\rm light}, n_{\rm heavy}) = (1, 3)$. This table is originally shown in [14].

$\Delta c_F = 0.04$

z_L	θ_H	m_{F_l} (TeV)	$m_{Z_R^{(1)}}$ (TeV)	σ_N (cm^2)
4×10^4	0.097	2.29	6.47	2.69×10^{-44}
3×10^4	0.092	2.46	6.74	2.35×10^{-44}
2×10^4	0.085	2.72	7.15	1.96×10^{-44}
10^4	0.074	3.24	7.92	1.53×10^{-44}

$\Delta c_F = 0.06$

z_L	θ_H	m_{F_l} (TeV)	$m_{Z_R^{(1)}}$ (TeV)	σ_N (cm^2)
2×10^4	0.085	2.61	7.15	1.76×10^{-44}
10^4	0.074	3.13	7.92	1.35×10^{-44}

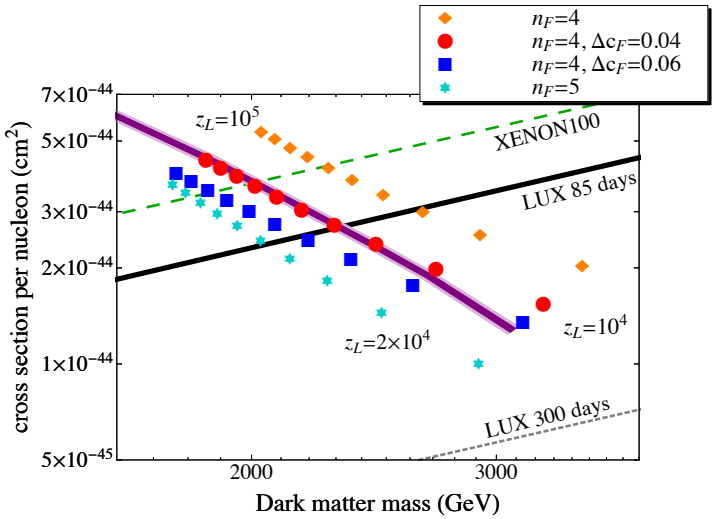

Figure 28: The spin-independent cross section of the F^0-nucleon elastic scattering for $10^4 \leq z_L \leq 10^5$. The orange diamonds and light blue stars represent the $n_F = 4$ and $n_F = 5$ cases of degenerate dark fermions with a step of 10^4 in z_L, respectively. Red circles and blue squares represent the cases of non-degenerate dark fermions $(n_{\rm light}, n_{\rm heavy}) = (1, 3)$ with $\Delta c_F = 0.04$ and 0.06, respectively. The black solid line and green dashed line are the 90% confidence limits set by the 85.3 live-days result of the LUX experiment[33] and the 225 live-days result of the XENON100 experiment[32], respectively. The purple and light purple bands represent the regions allowed by the limit of the relic density of DM at the 68 % CL depicted in Fig. 26 and by twice of that. The model with dark fermions of $2.3\,{\rm TeV} < m_{F_l} < 3.1\,{\rm TeV}$ $(4 \times 10^4 > z_L > 10^4)$ gives a consistent scenario. This figure is originally shown in [14].

7 Conclusion

In this paper we constructed and analyzed the SO(5)×U(1) gauge-Higgs unification with Higgs mass $m_H = 126$ GeV. The $SO(5) \times U(1)$ GHU has $\mathrm{SU}(3)_C \times \mathrm{SO}(5) \times \mathrm{U}(1)_X$ gauge symmetry on the Randall-Sundrum warped space-time. The four dimensional Higgs boson appears a part of the extra dimensional component of the $SO(5)$ gauge fields. The quark and leptons are introduced in the vectorial representation of $SO(5)$. To realize the observed unstable Higgs boson, the dark fermions are introduced in the spinorial representation of $SO(5)$. The four dimensional Higgs boson appears as the fluctuation mode of the AB phase θ_H. This phase is determined by location of the global minimum of the effective potential $V_{\rm eff}(\theta_H)$. When the effective potential is determined, the relevant parameters were determined self-consistently. The Higgs mass and Higgs cubic and quartic couplings are determined by $V_{\rm eff}(\theta_H)$. The shape of $V_{\rm eff}(\theta_H)$ strongly depends on the detail of the gauge boson, top quark multiplet and dark fermion sector.

We determined parameter sets for $m_H = 126$ GeV. We demonstrated how to determine the relevant parameters. We fixed warp factor z_L and the number of the dark fermions n_F and chose the global minimum θ_1 in the effective potential tentatively. Then we calculated the other relevant parameters and determined the Higgs mass. If the obtained Higgs mass was smaller (larger) than 126 GeV, we reiterated the same procedure with smaller (larger) θ_1. After we determined the relevant parameters, the global minimum θ_H was determined and all other quantities such as the mass spectra of all KK towers, gauge couplings of all particles, and Yukawa couplings of all fermions were determined. In the case of $n_F = 1, 2$ and 3, small z_L cannot reproduce $m_H = 126$ GeV because the small z_L gives $m_H < 126$ GeV. In the case of $n_F \geq 4$ and $z_L < 10^4$, this case cannot reproduce the top mass.

The fact $m_H = 126$ GeV leads to important consequences in the $SO(5) \times U(1)$ GHU. We found the universal relations which are independent on the detail of the dark fermions. The universal relations appear among θ_H, the KK mass, the masses of $Z_R^{(1)}$, $Z^{(1)}$, $\gamma^{(1)}$ and $t^{(1)}$, couplings $Z^{(1)}\bar{q}q$, the Higgs cubic and quartic couplings. If one finds the value of $m_{Z^{(1)}}(\theta_H)$ from experiments, θ_H is determined and other quantities are predicted. And we can know the behavior of the KK mass and couplings at the SM limit ($\theta_H \to 0$) without informations of the dark fermions, although, strictly speaking, we cannot take $\theta \to 0$ limit. Especially our Higgs cubic and quartic couplings are smaller than those in the SM.

In Sec.5.1, we estimated θ_H region which is consistent with the LHC experiments. Firstly we analyzed Higgs decay $H \to \gamma\gamma$. The infinite sum of the KK modes in the loop corrections converges. The KK mode contributions to the branching fraction are 0.2% (2%) for $\theta_H = 0.117$ (0.360). Because the Higgs couplings in the $SO(5) \times U(1)$ GHU have the factor $\cos\theta_H$ compared to the SM. Higgs production rate is suppressed by $\cos^2\theta_H$ compared to the SM. The branching fraction is almost the same as that in the SM. Therefore in signal strength dominant factor of deviation from the SM is $\cos^2\theta_H$. For $\theta_H = 0.1\,(0.3)$ the signal strength is also about 0.99 (0.91) compared to the SM. Secondary we examined the prediction of KK particles at LHC experiments. First exited KK modes of Z boson $Z^{(1)}$, photon $\gamma^{(1)}$, the lowest mode of Z_R and $Z_R^{(1)}$ have TeV scale mass in the $SO(5)\times U(1)$ GHU. These massive neutral gauge bosons become Z' boson. In the $SO(5) \times U(1)$ GHU Z' bosons is strongly coupled with right handed fermions so that Z' bosons have large width. The decay widths of $Z_R^{(1)}$, $Z^{(1)}$ and $\gamma^{(1)}$ are 482, 342 and 886 GeV (553, 494 GeV and 1.04 TeV) for $\theta_H = 0.114$ (0.073). The region $\theta_H < 0.13$ ($m_{Z_R^{(1)}} >$5.1 TeV) in our model is consistent with the result of Z' search in the LHC experiments. We predicted Z' are discovered in the 14 TeV LHC experiments.

In addition to the collider experiments we examined the implication of a dark matter problem. The dark fermions with $Q_X = 1/2$ have the neutral and charged components. The charged dark fermion is heavier than the neutral one due to the radiative correction. In the $SO(5) \times U(1)$ GHU the number of dark fermions is conserved and the lightest dark fermions become stable. We evaluated the relic density of the dark matter. In the degenerate case, it turns out that the observed relic density is not reproduced. We found that we can reconstruct the relic density with the case of $(n_{\rm light}, n_{\rm heavy}) = (1, 3)$. The relic density is consistent with the experimental bound for $10^4 \lesssim z_L \lesssim 10^6$, $0.04 \lesssim \Delta c_F \lesssim 0.07$ (400 GeV $< \Delta m_F <$ 500 GeV). We also examined the direct detection of the dark matter. We calculated the spin-independent scattering cross section of the lightest neutral dark fermions with nucleons. We found that in the region $10^4 \lesssim z_L \lesssim 4 \times 10^4$ for $(n_{\rm light}, n_{\rm heavy}) = (1, 3)$ our model is consistent with the result of the relic density and direct search from Planck, XENON100 and LUX experiments. The neutral dark fermion masses are favored in the region 3.1 TeV to 2.3 TeV (θ_H =0.074 - 0.097). Especially for the direct detection our model indicates dark matter is discovered in the next LUX experiments.

As we have seen, there exists the region which is consistent with the experiments of the relic density, direct search and the results of Higgs decay $H \to \gamma\gamma$ and Z' search.

θ_H ranges from 0.074 to 0.097. We predicted our Z' bosons a dark fermions should be observed by the upgraded LHC and LUX experiments in near future. It is interesting that the parameter regions in which Z' bosons and the dark fermions should be observed are overlapped. We note that suppose that the Z' bosons or the dark fermions in our model are observed. We can predict the Higgs cubic and quartic couplings through the θ_H with the universality. When θ_H ranges from 0.074 to 0.097, we can predict $\lambda_3 \sim 29$ GeV, $\lambda_4 \sim 0.021$, $m_{\text{top}^{(1)}} = 7.7 - 9.8$ TeV and $m_{Z_R^{(1)}} = 6.5 - 7.9$ TeV. When the Higgs self-couplings are measured by the future experiments, we can distinguish the gauge-Higgs unification from the other models which include the SM.

Acknowledgements I am very very grateful to my supervisor Prof. Yutaka Hosotani for his great advises, encouragements and discussions. I appreciate the discussion and the works with the collaborators, Shuichiro Funatsu, Hisaki Hatanaka, Yutaka Hosotani and Yuta Orikasa. And I also appreciate the works with the other collaborators, Akinori Tanaka and Akio Tomiya. I am thankful to Yutaka Hosotani, Koji Hashimoto, Kin-ya Oda, Masaharu Aoki and Minoru Tanaka for their great advises as five-member committee. I thank all members of particle physics theory group at Osaka University and all office workers in Osaka university. This work was supported in part by JSPS KAKENHI grants, No. 13J01861.

Appendices

A $Z\bar{q}q$ couplings

This section is originally shown in [13]. The couplings of $Z\bar{q}q$ is given by

$$
\begin{aligned}
Z_\mu^{(n)}(x)\, g_w\sqrt{L}\int_1^{z_L} dz \Big[& \bar{t}_L\gamma^\mu t_L(x)\Big\{\frac{1}{2}h^L_{Z^{(n)}}\left(f_{t_L}f_{t_L}+f_{U_L}f_{U_L}-f_{B_L}f_{B_L}\right) \\
& +\frac{1}{2}h^R_{Z^{(n)}}\left(f_{B_L}f_{B_L}+f_{U_L}f_{U_L}-f_{t_L}f_{t_L}\right)+\hat{h}_{Z^{(n)}}\left(f_{B_L}f_{t'_L}+f_{t_L}f_{t'_L}\right) \\
& +\frac{g_B}{3g_A}h^B_{Z^{(n)}}\left(2f_{B_L}f_{B_L}+2f_{t_L}f_{t_L}+2f_{t'_L}f_{t'_L}-f_{U_L}f_{U_L}\right)\Big\} \\
& +\bar{b}_L\gamma^\mu b_L(x)\Big\{\frac{1}{2}h^L_{Z^{(n)}}\left(f_{X_L}f_{X_L}-f_{b_L}f_{b_L}-f_{D_L}f_{D_L}\right) \\
& +\frac{1}{2}h^R_{Z^{(n)}}\left(f_{D_L}f_{D_L}-f_{X_L}f_{X_L}-f_{b_L}f_{b_L}\right)+\hat{h}_{Z^{(n)}}\left(f_{D_L}f_{b'_L}-f_{X_L}f_{b'_L}\right) \\
& +\frac{g_B}{3g_A}h^B_{Z^{(n)}}\left(f_{b_L}f_{b_L}-f_{D_L}f_{D_L}-f_{b'_L}f_{b'_L}-f_{X_L}f_{X_L}\right)\Big\}\Big]
\end{aligned}
$$

$$+(L \to R)\ . \tag{A.1}$$

where fs and hs are defined by followings.

The mode functions of the Z tower are

$$\begin{pmatrix} h^L_{Z^{(n)}}(z) \\ h^R_{Z^{(n)}}(z) \\ \hat{h}_{Z^{(n)}}(z) \\ h^B_{Z^{(n)}} \end{pmatrix} = \frac{1}{\sqrt{1+s_\phi^2}} \frac{1}{\sqrt{2\, r_{Z^{(n)}}}} \begin{pmatrix} \left\{(1+s_\phi^2)(1+\cos\theta_H) - 2s_\phi^2\right\} C(z;\lambda_{Z^{(n)}}) \\ \left\{(1+s_\phi^2)(1-\cos\theta_H) - 2s_\phi^2\right\} C(z;\lambda_{Z^{(n)}}) \\ -\sqrt{2}(1+s_\phi^2)\sin\theta_H \hat{S}(z;\lambda_{Z^{(n)}}) \\ -2s_\phi c_\phi C(z;\lambda_{Z^{(n)}}) \end{pmatrix},$$

$$\begin{aligned} r_{Z^{(n)}} = \int_1^{z_L} \frac{dz}{kz} \Big\{ & c_\phi^2 C(z;\lambda_{Z^{(n)}})^2 \\ & + (1+s_\phi^2)[\cos^2\theta_H C(z;\lambda_{Z^{(n)}})^2 + \sin^2\theta_H \hat{S}(z;\lambda_{Z^{(n)}})^2 \Big\}. \end{aligned} \tag{A.2}$$

Wave functions for the KK tower of an up-type quark t (top) are given by

$$\begin{pmatrix} U_L(x,z) \\ B_L(x,z) \\ t_L(x,z) \\ t'_L(x,z) \end{pmatrix} \supset \frac{\sqrt{k}z^2}{\sqrt{r_{t^{(n)}}}} \begin{pmatrix} a_U^{(n)} C_L^{(2)}(z,\lambda_{t^{(n)}}) \\ a_B^{(n)} C_L^{(1)}(z,\lambda_{t^{(n)}}) \\ a_t^{(n)} C_L^{(1)}(z,\lambda_{t^{(n)}}) \\ a_{t'}^{(n)} S_L^{(1)}(z,\lambda_{t^{(n)}}) \end{pmatrix} t_L^{(n)}(x) \equiv \sqrt{k}z^2 \begin{pmatrix} f_{U_L}^{(n)}(z) \\ f_{B_L}^{(n)}(z) \\ f_{t_L}^{(n)}(z) \\ f_{t'_L}^{(n)}(z) \end{pmatrix} t_L^{(n)}(x)\ ,$$

$$\begin{pmatrix} U_R(x,z) \\ B_R(x,z) \\ t_R(x,z) \\ t'_R(x,z) \end{pmatrix} \supset \frac{\sqrt{k}z^2}{\sqrt{r_{t^{(n)}}}} \begin{pmatrix} a_U^{(n)} S_R^{(2)}(z,\lambda_{t^{(n)}}) \\ a_B^{(n)} S_R^{(1)}(z,\lambda_{t^{(n)}}) \\ a_t^{(n)} S_R^{(1)}(z,\lambda_{t^{(n)}}) \\ a_{t'}^{(n)} C_R^{(1)}(z,\lambda_{t^{(n)}}) \end{pmatrix} t_R^{(n)}(x) \equiv \sqrt{k}z^2 \begin{pmatrix} f_{U_R}^{(n)}(z) \\ f_{B_R}^{(n)}(z) \\ f_{t_R}^{(n)}(z) \\ f_{t'_R}^{(n)}(z) \end{pmatrix} t_R^{(n)}(x)\ ,$$

$$\begin{aligned} r_{t^{(n)}} &= \int_1^{z_L} dz \Big\{ a_U^{(n)2} C_L^{(2)}(z,\lambda_{t^{(n)}})^2 + (a_B^{(n)2} + a_t^{(n)2}) C_L^{(1)}(z,\lambda_{t^{(n)}})^2 + a_{t'}^{(n)2} S_L^{(1)}(z,\lambda_{t^{(n)}})^2 \Big\} \\ &= \int_1^{z_L} dz \Big\{ a_U^{(n)2} S_R^{(2)}(z,\lambda_{t^{(n)}})^2 + (a_B^{(n)2} + a_t^{(n)2}) S_R^{(1)}(z,\lambda_{t^{(n)}})^2 + a_{t'}^{(n)2} C_R^{(1)}(z,\lambda_{t^{(n)}})^2 \Big\}. \end{aligned} \tag{A.3}$$

Here $C_L^{(i)}(z,\lambda_{t^{(n)}}) = C_L(z;\lambda_{t^{(n)}},c_i)$, $S_R^{(i)}(z,\lambda_{b^{(n)}}) = S_R(z;\lambda_{b^{(n)}},c_i)$, etc., and other towers of $Q_{\rm EM} = \frac{2}{3}e$ fermions have been suppressed. The common factors are given by

$$\begin{pmatrix} a_U^{(n)} \\ a_B^{(n)} \\ a_t^{(n)} \\ a_{t'}^{(n)} \end{pmatrix} = \begin{pmatrix} -\sqrt{2}\tilde{\mu}^q C_L^{(1)}/\mu_2^q C_L^{(2)} \\ (1-\cos\theta_H)/\sqrt{2} \\ (1+\cos\theta_H)/\sqrt{2} \\ -\sin\theta_H C_L^{(1)}/S_L^{(1)} \end{pmatrix},$$

$$C_L^{(i)} \equiv C_L(1;\lambda_{t^{(n)}},c_i)\ ,\quad S_L^{(i)} \equiv S_L(1;\lambda_{t^{(n)}},c_i)\ , \tag{A.4}$$

where $\lambda_{t^{(n)}}$ satisfies (3.38).

For a down-type quark b (bottom) we have

$$\begin{pmatrix} b_L(x,z) \\ X_L(x,z) \\ D_L(x,z) \\ b'_L(x,z) \end{pmatrix} \supset \frac{\sqrt{k}z^2}{\sqrt{r_{b^{(n)}}}} \begin{pmatrix} a_b^{(n)} C_L^{(1)}(z,\lambda_{b^{(n)}}) \\ a_X^{(n)} C_L^{(2)}(z,\lambda_{b^{(n)}}) \\ a_D^{(n)} C_L^{(2)}(z,\lambda_{b^{(n)}}) \\ a_{b'}^{(n)} S_L^{(2)}(z,\lambda_{b^{(n)}}) \end{pmatrix} b_L^{(n)}(x) \equiv \sqrt{k}z^2 \begin{pmatrix} f_{b_L}^{(n)}(z) \\ f_{X_L}^{(n)}(z) \\ f_{D_L}^{(n)}(z) \\ f_{b'_L}^{(n)}(z) \end{pmatrix} b_L^{(n)}(x) \ ,$$

$$\begin{pmatrix} b_R(x,z) \\ X_R(x,z) \\ D_R(x,z) \\ b'_R(x,z) \end{pmatrix} \supset \frac{\sqrt{k}z^2}{\sqrt{r_{b^{(n)}}}} \begin{pmatrix} a_b^{(n)} S_R^{(1)}(z,\lambda_{b^{(n)}}) \\ a_X^{(n)} S_R^{(2)}(z,\lambda_{b^{(n)}}) \\ a_D^{(n)} S_R^{(2)}(z,\lambda_{b^{(n)}}) \\ a_{b'}^{(n)} C_R^{(2)}(z,\lambda_{b^{(n)}}) \end{pmatrix} b_R^{(n)}(x) \equiv \sqrt{k}z^2 \begin{pmatrix} f_{b_R}^{(n)}(z) \\ f_{X_R}^{(n)}(z) \\ f_{D_R}^{(n)}(z) \\ f_{b'_R}^{(n)}(z) \end{pmatrix} b_R^{(n)}(x) \ ,$$

$$\begin{pmatrix} a_b^{(n)} \\ a_X^{(n)} \\ a_D^{(n)} \\ a_{b'}^{(n)} \end{pmatrix} = \begin{pmatrix} -\sqrt{2}\mu_2^q C_L^{(2)}/\tilde{\mu}^q C_L^{(1)} \\ (1-\cos\theta_H)/\sqrt{2} \\ (1+\cos\theta_H)/\sqrt{2} \\ \sin\theta_H C_L^{(2)}/S_L^{(2)} \end{pmatrix},$$

$$C_L^{(i)} \equiv C_L(1;\lambda_{b^{(n)}},c_i), \quad S_L^{(i)} \equiv S_L(1;\lambda_{b^{(n)}},c_i) \ ,$$

$$\begin{aligned} r_{b^{(n)}} &= \int_1^{z_L} dz \Big\{ a_b^{(n)2} C_L^{(1)}(z,\lambda_{b^{(n)}})^2 + (a_X^{(n)2} + a_D^{(n)2}) C_L^{(2)}(z,\lambda_{b^{(n)}})^2 + a_{b'}^{(n)2} S_L^{(2)}(z,\lambda_{b^{(n)}})^2 \Big\} \\ &= \int_1^{z_L} dz \Big\{ a_b^{(n)2} S_R^{(1)}(z,\lambda_{b^{(n)}})^2 + (a_X^{(n)2} + a_D^{(n)2}) S_R^{(2)}(z,\lambda_{b^{(n)}})^2 + a_{b'}^{(n)2} C_R^{(2)}(z,\lambda_{b^{(n)}})^2 \Big\}. \end{aligned} \tag{A.5}$$

where $\lambda_{b^{(n)}}$ satisfies (3.39).

B Generators and the Wilson line phase

We define the generators of $SU(2)'_L$ and $SU(2)'_R$ as S^{a_L,a_R} which appears after the electroweak symmetry breaking,

$$S^{a_L} = \alpha T^{a_L} + \beta T^{a_R} + \gamma T^{\hat{a}}, \tag{B.1}$$

where T^{a_L}, T^{a_R} and $T^{\hat{a}}$ are $SO(5)$ generators. Coefficients α, β and γ are determined by algebra $[S_L^a, S_L^b] = i\epsilon^{abc}$,

$$\begin{aligned} \alpha^2 + \tfrac{\gamma^2}{2} &= \alpha \\ \beta^2 + \tfrac{\gamma^2}{2} &= \beta \\ (\alpha+\beta)\gamma &= \gamma. \end{aligned} \tag{B.2}$$

Then we get,

$$\begin{aligned}\alpha &= \tfrac{1}{2}(1+\cos\theta)\\ \beta &= \tfrac{1}{2}(1-\cos\theta)\\ \gamma &= \tfrac{1}{\sqrt{2}}\sin\theta,\end{aligned} \tag{B.3}$$

where θ is the parameter in the region $\theta = 0$ - 2π. $SU(2)'_R$ generators S^{a_R} is orthogonal to $SU(2)'_L$. This θ is corresponding to θ_H. The coefficient of $T^{1_L} + T^{2_L}$ is $(1+\cos\theta)/2$ which is the same of θ_H dependence of W boson mode function. We can also construct the Z boson generators (A.2). These relations $(B.3)$ can be derived by another way. Suppose we define unitary transformation $\Omega = e^{i\alpha T^{\hat{4}}}$,

$$\begin{aligned}S^{a_L} &= \Omega(\alpha)T^{a_L}\Omega^{-1}(\alpha) \equiv T^{a_L}(\alpha)\\ S^{a_R} &= \Omega(\alpha)T^{a_R}\Omega^{-1}(\alpha) \equiv T^{a_R}(\alpha)\\ S^{\hat{a}} &= \Omega(\alpha)T^{\hat{a}}\Omega^{-1}(\alpha) \equiv T^{\hat{a}}(\alpha),\end{aligned} \tag{B.4}$$

where $S^{\hat{a}}$ are $SO(5)/SO(4)'$ generators. We solve these equations and redefine $\theta = \alpha/\sqrt{2} - \pi$. We can get eq.$(B.3)$ again. This means Wilson line phase rotates the axis of the symmetry by unitary transformation. When the symmetry is broken by Wilson line phase, we should consider this rotation.

C Calculation of effective potential

We can evaluate d dimensional 1-loop Higgs effective potential from the mass spectrums,

$$V_{\text{eff}} = \frac{1}{(4\pi)^{d/2}\Gamma(\frac{d}{2})}\int_0^\infty dy\, y^{d-1}\ln\rho(iy) \tag{C.1}$$

where ρ is mass spectrum function which is satisfied $\rho(m) = 0$. Let us first consider 1-loop effective potential with KK spectrum $m_n(\theta_H)$,

$$\begin{aligned}V_{\text{eff}} &= \tfrac{1}{2}\textstyle\int \frac{d^4p_E}{(2\pi)^4}\sum_n \ln\left(p_E^2 + m_n^2\right),\\ m_n^2 &\sim \left(\tfrac{n+a}{R}\right)^2.\end{aligned} \tag{C.2}$$

We ignore the positive sign for bosons and the negative sign for fermions in this formula. We define a function,

$$f(\Delta) \equiv \int \frac{d^dp}{(2\pi)^d}\ln\left(p^2+\Delta\right).$$

We differentiate this function with Δ,

$$\begin{aligned}\frac{d}{d\Delta}f(\Delta) &= \int \frac{d^dp}{(2\pi)^d}\frac{1}{p^2+\Delta}, \\ &= \frac{\Gamma(1-\frac{d}{2})}{(4\pi)^{d/2}}\frac{1}{\Delta^{1-d/2}}.\end{aligned} \tag{C.3}$$

We integrate from zero to Δ,

$$f(\Delta)-f(0) = \frac{2}{d}\frac{\Gamma(1-\frac{d}{2})}{(4\pi)^{d/2}}\Delta^{\frac{d}{2}}. \tag{C.4}$$

Therefore, we get the effective potential with only a dependent θ_H part,

$$V_{\rm eff} = \frac{1}{d}\frac{\Gamma(1-\frac{d}{2})}{(4\pi)^{d/2}}\sum_n m_n^d \tag{C.5}$$

Next, we consider to evaluate $\sum_n m_n^d$. We define spectral function $\rho(z)$ which is analytic on the complex plane and is satisfied $\rho(m_n)=0$ on the real axis. For example, ρ is

$$\rho(z)\sim a_n(z-m_n), \qquad \frac{\rho'(z)}{\rho(z)}\sim\frac{1}{z-m_n}. \tag{C.6}$$

We integrate all $m_n(\theta_H)$ on $\mathrm{Re}\, z>0$ along a contour C,

$$\int_C dz\, z^d\frac{\rho'(z)}{\rho(z)} = \sum_n -2\pi i\, m_n^d. \tag{C.7}$$

Let us estimate the left side of this equation,

$$\begin{aligned}\sum_n m_n^d &= -\frac{1}{2\pi i}\int_C dz\, z^d\frac{\rho'(z)}{\rho(z)}, \\ &= \frac{d}{2\pi i}\int_C dz\, z^{d-1}\ln\rho(z).\end{aligned} \tag{C.8}$$

Suppose this integral is satisfied with $|z^{d-1}\ln\rho| < 1/R$ for $|z|\to\infty$. We can integrate along the imaginary axis,

$$\begin{aligned}\sum_n m_n^d &= \frac{d}{2\pi i}\int_{C'} dz\, z^{d-1}\ln\rho(z), \\ &= \frac{d}{2\pi i}\left(\int_{C'_-}+\int_{C'_+}\right) dz\, z^{d-1}\ln\rho(z),\end{aligned} \tag{C.9}$$

where Contours C'_- and C'_+ are negative value of $\mathrm{Im}z$ and positive value of $\mathrm{Im}z$, respectively,

$$\begin{aligned}C'_+ :&\quad z=iy, \quad y:0\to\infty, \\ C'_- :&\quad z=-iy, \ \ y:\infty\to 0.\end{aligned} \tag{C.10}$$

When the ρ is even function $\rho(iy) = \rho(-iy)$,

$$\begin{aligned}\sum_n m_n^d &= \frac{d}{2\pi i}\left\{e^{\frac{\pi}{2}id}\int_0^\infty dy\, y^{d-1}\ln\rho(iy) + e^{-\frac{\pi}{2}id}\int_\infty^0 dy\, y^{d-1}\ln\rho(-iy)\right\}, \\ &= \frac{d}{2\pi i}2i\sin\frac{\pi d}{2}\int_0^\infty dy\, y^{d-1}\ln\rho(iy). \end{aligned} \tag{C.11}$$

Therefore,

$$\begin{aligned}V_{\text{eff}} &= \frac{\Gamma(1-\frac{d}{2})}{(4\pi)^{d/2}}\frac{1}{\pi}\sin\frac{\pi d}{2}\int_0^\infty dy\, y^{d-1}\ln\rho(iy), \\ &= \frac{1}{(4\pi)^{d/2}\Gamma(\frac{d}{2})}\int_0^\infty dy\, y^{d-1}\ln\rho(iy). \end{aligned} \tag{C.12}$$

where we use the formula of gamma function,

$$\Gamma\left(\frac{d}{2}\right)\Gamma\left(1-\frac{d}{2}\right) = \frac{\pi}{\sin\frac{\pi d}{2}}. \tag{C.13}$$

References

[1] G. Aad *et al.* [ATLAS Collaboration], "Observation of a new particle in the search for the Standard Model Higgs boson with the ATLAS detector at the LHC," Phys. Lett. B **716**, 1 (2012) [arXiv:1207.7214 [hep-ex]].

[2] S. Chatrchyan *et al.* [CMS Collaboration], "Observation of a new boson at a mass of 125 GeV with the CMS experiment at the LHC," Phys. Lett. B **716**, 30 (2012) [arXiv:1207.7235 [hep-ex]].

[3] G. Aad *et al.* [ATLAS Collaboration], "Measurement of the Higgs boson mass from the $H \to \gamma\gamma$ and $H \to ZZ^* \to 4\ell$ channels with the ATLAS detector using 25 fb^{-1} of pp collision data," Phys. Rev. D **90**, 052004 (2014) [arXiv:1406.3827 [hep-ex]].

[4] Y. Hosotani, "Dynamical Mass Generation by Compact Extra Dimensions," *Phys.Lett.* **B126** (1983) 309.

[5] Y. Hosotani, "Dynamics of Nonintegrable Phases and Gauge Symmetry Breaking," *Annals Phys.* **190** (1989) 233.

[6] H. Hatanaka, T. Inami, and C. Lim, "The Gauge hierarchy problem and higher dimensional gauge theories," *Mod.Phys.Lett.* **A13** (1998) 2601–2612, `arXiv:hep-th/9805067 [hep-th]`.

[7] S. Funatsu, H. Hatanaka, Y. Hosotani, Y. Orikasa and T. Shimotani, "Novel universality and Higgs decay $H \to \gamma\gamma, gg$ in the $SO(5) \times U(1)$ gauge-Higgs unification," Phys. Lett. B **722**, 94 (2013) [arXiv:1301.1744 [hep-ph]].

[8] K. Agashe, R. Contino, and A. Pomarol, "The Minimal composite Higgs model," *Nucl.Phys.* **B719** (2005) 165–187, `arXiv:hep-ph/0412089 [hep-ph]`.

[9] A. D. Medina, N. R. Shah, and C. E. Wagner, "Gauge-Higgs Unification and Radiative Electroweak Symmetry Breaking in Warped Extra Dimensions," *Phys.Rev.* **D76** (2007) 095010, `arXiv:0706.1281 [hep-ph]`.

[10] Y. Hosotani, K. Oda, T. Ohnuma, and Y. Sakamura, "Dynamical Electroweak Symmetry Breaking in SO(5) x U(1) Gauge-Higgs Unification with Top and Bottom Quarks," *Phys.Rev.* **D78** (2008) 096002, `arXiv:0806.0480 [hep-ph]`.

[11] M. Serone, "Holographic Methods and Gauge-Higgs Unification in Flat Extra Dimensions," *New J.Phys.* **12** (2010) 075013, `arXiv:0909.5619 [hep-ph]`.

[12] Y. Hosotani, S. Noda, and N. Uekusa, "The Electroweak gauge couplings in SO(5) x U(1) gauge-Higgs unification," *Prog.Theor.Phys.* **123** (2010) 757–790, `arXiv:0912.1173 [hep-ph]`.

[13] S. Funatsu, H. Hatanaka, Y. Hosotani, Y. Orikasa and T. Shimotani, "LHC signals of the $SO(5) \times U(1)$ gauge-Higgs unification," Phys. Rev. D **89**, 095019 (2014) [arXiv:1404.2748 [hep-ph]].

[14] S. Funatsu, H. Hatanaka, Y. Hosotani, Y. Orikasa and T. Shimotani, "Dark matter in the SO(5) $\times$ U(1) gauge-Higgs unification," PTEP **2014**, no. 11, 113B01 (2014) [arXiv:1407.3574 [hep-ph]].

[15] L. Randall and R. Sundrum, "A Large mass hierarchy from a small extra dimension," Phys. Rev. Lett. **83**, 3370 (1999) [hep-ph/9905221].

[16] J. Beringer *et al.* [Particle Data Group Collaboration], "Review of Particle Physics (RPP)," Phys. Rev. D **86**, 010001 (2012).

[17] N. Haba, Y. Sakamura and T. Yamashita, "Tree-level unitarity in Gauge-Higgs Unification," JHEP **1003**, 069 (2010) [arXiv:0908.1042 [hep-ph]].

[18] CMS Collaboration [CMS Collaboration], "Search for multi-charged Heavy Stable Charged Particles," CMS-PAS-EXO-11-090.

[19] G. Aad *et al.* [ATLAS Collaboration], "Search for long-lived, multi-charged particles in pp collisions at $\sqrt{s}$=7 TeV using the ATLAS detector," Phys. Lett. B **722**, 305 (2013) [arXiv:1301.5272 [hep-ex]].

[20] G. Aad *et al.* [ATLAS Collaboration], "Measurement of Higgs boson production in the diphoton decay channel in *pp* collisions at center-of-mass energies of 7 and 8 TeV with the ATLAS detector," Phys. Rev. D **90**, 112015 (2014) [arXiv:1408.7084 [hep-ex]].

[21] V. Khachatryan *et al.* [CMS Collaboration], "Observation of the diphoton decay of the Higgs boson and measurement of its properties," Eur. Phys. J. C **74**, no. 10, 3076 (2014) [arXiv:1407.0558 [hep-ex]].

[22] J. R. Ellis, M. K. Gaillard and D. V. Nanopoulos, "A Phenomenological Profile of the Higgs Boson," Nucl. Phys. B **106**, 292 (1976).

[23] M. A. Shifman, A. I. Vainshtein, M. B. Voloshin and V. I. Zakharov, "Low-Energy Theorems for Higgs Boson Couplings to Photons," Sov. J. Nucl. Phys. **30**, 711 (1979) [Yad. Fiz. **30**, 1368 (1979)].

[24] J. F. Gunion, H. E. Haber, G. L. Kane and S. Dawson, "The Higgs Hunter's Guide," Front. Phys. **80**, 1 (2000).

[25] H. M. Georgi, S. L. Glashow, M. E. Machacek and D. V. Nanopoulos, "Higgs Bosons from Two Gluon Annihilation in Proton Proton Collisions," Phys. Rev. Lett. **40**, 692 (1978).

[26] S. Dawson, "Radiative corrections to Higgs boson production," Nucl. Phys. B **359**, 283 (1991).

[27] M. Spira, A. Djouadi, D. Graudenz and P. M. Zerwas, "Higgs boson production at the LHC," Nucl. Phys. B **453**, 17 (1995) [hep-ph/9504378].

[28] J. Alcaraz *et al.* [ALEPH and DELPHI and L3 and OPAL and LEP Electroweak Working Group Collaborations], "A Combination of preliminary electroweak measurements and constraints on the standard model," hep-ex/0612034.

[29] G. Aad *et al.* [ATLAS Collaboration], "Search for high-mass dilepton resonances in pp collisions at $\sqrt{s} = 8$ TeV with the ATLAS detector," Phys. Rev. D **90**, no. 5, 052005 (2014) [arXiv:1405.4123 [hep-ex]].

[30] V. Khachatryan *et al.* [CMS Collaboration], "Search for physics beyond the standard model in dilepton mass spectra in proton-proton collisions at $\sqrt{s} = 8$ TeV," arXiv:1412.6302 [hep-ex].

[31] P. A. R. Ade *et al.* [Planck Collaboration], "Planck 2013 results. XVI. Cosmological parameters," Astron. Astrophys. **571**, A16 (2014) [arXiv:1303.5076 [astro-ph.CO]].

[32] E. Aprile *et al.* [XENON100 Collaboration], "Dark Matter Results from 225 Live Days of XENON100 Data," Phys. Rev. Lett. **109**, 181301 (2012) [arXiv:1207.5988 [astro-ph.CO]].

[33] D. S. Akerib *et al.* [LUX Collaboration], "First results from the LUX dark matter experiment at the Sanford Underground Research Facility," Phys. Rev. Lett. **112**, no. 9, 091303 (2014) [arXiv:1310.8214 [astro-ph.CO]].

[34] K. Griest and D. Seckel, "Three exceptions in the calculation of relic abundances," Phys. Rev. D **43**, 3191 (1991).

[35] E. W. Kolb and M. S. Turner, "The Early Universe," Front. Phys. **69**, 1 (1990).

[36] G. Servant and T. M. P. Tait, "Is the lightest Kaluza-Klein particle a viable dark matter candidate?," Nucl. Phys. B **650**, 391 (2003) [hep-ph/0206071].

[37] G. Jungman, M. Kamionkowski and K. Griest, "Supersymmetric dark matter," Phys. Rept. **267**, 195 (1996) [hep-ph/9506380].

[38] J. R. Ellis, A. Ferstl and K. A. Olive, "Reevaluation of the elastic scattering of supersymmetric dark matter," Phys. Lett. B **481**, 304 (2000) [hep-ph/0001005].

[39] M. W. Goodman and E. Witten, "Detectability of Certain Dark Matter Candidates," Phys. Rev. D **31**, 3059 (1985).

[40] S. Durr, Z. Fodor, T. Hemmert, C. Hoelbling, J. Frison, S. D. Katz, S. Krieg and T. Kurth *et al.*, "Sigma term and strangeness content of octet baryons," Phys. Rev. D **85**, 014509 (2012) [arXiv:1109.4265 [hep-lat]].

[41] Y. Hosotani and Y. Kobayashi, "Yukawa Couplings and Effective Interactions in Gauge-Higgs Unification," Phys. Lett. B **674**, 192 (2009) [arXiv:0812.4782 [hep-ph]].